DISTINCT LYSOSOMAL DYSFUNCTION PATTERNS OF PROGRANULIN DEFICIENCY IN THE CNS IMPLICATE PROGRANULIN IN CELL TYPE-SPECIFIC PROTEIN SORTING

Gordon C Werthmann[1,2,5] and Joachim Herz[1,2,3,4,6]

[1] Department of Molecular Genetics, University of Texas Southwestern Medical Center, Dallas, TX, USA.

[2] Center for Translational Neurodegeneration Research, Dallas, TX, USA.

[3] Department of Neuroscience, University of Texas Southwestern Medical Center, Dallas, TX, USA.

[4] Department of Neurology and Neurotherapeutics, University of Texas Southwestern Medical Center, Dallas, TX, USA.

[5] Corresponding author: gwerthmann@mgb.org

[6]Corresponding author: Joachim.herz@utsouthwestern.edu

Keywords: Neurodegeneration, Neural Ceroid Lipofuscinosis, Frontotemporal Lobar Degeneration, Lysosomal Proteome, Endo-lysosomal Dysfunction

Abstract

Loss-of-function mutations in Progranulin *(GRN)* cause neuronal ceroid lipofuscinosis (NCL) and hereditary frontotemporal dementia, presumably through lysosomal dysfunction. The effect of progranulin deficiency on cell type-specific lysosomal composition in the mammalian brain has not been examined. We used cell type-specific LysoIP to perform tandem-mass-tag mass-spectrometry and detected distinct aberrant proteomic signatures in progranulin-deficient astrocytes, neurons, and microglia, indicating cell type-specific dysregulation of key lysosomal proteins with crucial functions in sphingolipid metabolism and lysosome organization. These proteins markedly differed from progranulin-deficient RNAseq data sets, suggesting progranulin regulates lysosomal composition through post-translational mechanisms including the sorting of nascent proteins to the lysosome. Validation experiments confirmed that Mfsd8 and Ppt1, proteins whose mutation on their own cause NCL, were essentially absent from progranulin-deficient neuronal and microglial lysosomes, respectively. Our findings suggest that progranulin may function as an essential hub protein during endolysosomal sorting and highlight the necessity of restoring stoichiometric levels of progranulin expression in the secretory pathway for the development of effective therapeutic strategies.

41 **Introduction**

42 Frontotemporal dementia (FTD) is the second most common form of pre-senile dementia
43 and presents with a myriad of symptoms including behavioral abnormalities, impaired executive
44 function, and aphasia [1, 2]. Up to 40% of FTD cases are thought to be inherited, and
45 haploinsufficiency of the *GRN* gene on chromosome 17 is one of the most common causes of
46 familial FTD, termed GRN-FTD [3, 4]. Patients with GRN-FTD primarily develop the behavioral
47 variant of FTD, and on autopsy, the brains of these patients commonly contain TDP-43
48 aggregates. *GRN* codes for the protein progranulin, a lysosome resident protein comprised of 7
49 disulfide bond-rich, full length granulin domains and an N-terminal half-granulin domain. While
50 targeted to the lysosome through various membrane protein interactions [5, 6], progranulin is also
51 known to be secreted into the extracellular space where it is either cleaved into individual
52 granulins or endocytosed and delivered to the lysosome through the endocytic pathway [7, 8].

53 While haploinsufficiency of *GRN* leads to GRN-FTD, homozygous loss of progranulin
54 leads to a classic lysosomal storage disorder termed CLN11 (neuronal ceroid lipofuscinosis 11)
55 [9]. Unlike most proteins associated with lysosomal storage disorders, progranulin or granulins do
56 not appear to have any catalytic function and thus likely function as regulatory proteins within the
57 lysosome. The exact nature of how progranulin regulates the lysosomes, and why loss of
58 progranulin leads to a lysosomal storage disorder are currently unknown, but the links between
59 progranulin and lysosomal function are evident. Loss of progranulin leads to impaired cathepsin
60 D activity [10, 11], aberrant lysosomal lipid composition including decreased levels of the
61 lysosome-specific lipid BMP (bis(monoacylglycerol)phosphate), increased levels of tri-acyl
62 glycerol species [12-14], lysosomal alkalinization [15], and impaired lysosomal protein content *in*
63 *vitro* [16] and *in vivo* [17]. Progranulin deficiency also activates the CLEAR (coordinated lysosomal
64 expression and regulation) gene network by increasing the nuclear localization of the lysosomal
65 gene master regulator TFEB (transcription factor EB) [18, 19].

66 Progranulin has further been shown to regulate various cellular functions including neurite
67 outgrowth, immune regulation, and cell migration [20-24]. As both a resident lysosomal protein as
68 well as a secreted protein, the mechanism by which progranulin effects such a large range of
69 cellular processes has yet to be fully determined. However, previous work has demonstrated non-
70 secreted, lysosome-targeted progranulin recapitulates the excitotoxic protective effects of wild
71 type progranulin on cultured neurons [25]. This suggests the lysosomal function of progranulin is
72 – at least in part – responsible for the non-lysosomal effects of progranulin. Loss of progranulin
73 also leads to a proinflammatory phenotype. Progranulin deficient mice demonstrate microgliosis
74 and increased secretion of inflammatory cytokines such as C1qa and C3 [22]. *In vitro*, these
75 microglia are sufficient to induce aggregation of TDP-43 in co-cultured neurons [26].
76 How progranulin regulates lysosomal function remains to be understood; however,
77 previous work has demonstrated loss of progranulin leads to aberrations of the lysosomal
78 proteome, dysregulating key lysosomal proteins that are also implicated in lysosomal storage
79 disorders [16, 17]. To expand on this, we utilized a new technology termed LysoTag which allows
80 for the isolation of lysosomes *in vivo* in a cell type-specific manner in order to investigate the
81 effects of progranulin deficiency on the lysosomal proteome [27]. The specificity of this technique
82 allowed for precise isolation and investigation of the lysosomal proteome in progranulin-deficient
83 neurons, microglia, and astrocytes, revealing cell-type dependent protein aberrations not evident
84 upon whole brain analysis nor at the transcript level, and demonstrating the ability of progranulin
85 to regulate cell-specific lysosomal protein homeostasis in the mammalian brain.
86
87 **Results**
88
89 <u>LysoIP isolates lysosomes from specific cell types in *Grn* WT, Het, and KO mice</u>
90 In order to investigate the effects of progranulin deficiency on the lysosomal proteome *in*
91 *vivo*, we bred four specific Cre recombinase lines with previously defined TMEM192-3xHA fl/fl [27,

92 28] and *Grn* KO mouse lines [13]. These included *Ubc*-, *Syn*-, *Cx3cr1*-, and *Aldh1l1-Cre* lines for
93 pancellular, neuron-, microglia-, and astrocyte-specific LysoIP, respectively (Figure 1a). LysoIP
94 was performed on the brains of 2 to 3-month-old *Ubc*-, *Syn*-, and *Cx3cr1-Cre* mice or 6-month-
95 old *Aldh1l1-Cre* mice. 6-month-old *Aldh1l1-Cre* mice were used, because progranulin was
96 undetectable in any 3-month-old *Aldh1l1-Cre* mouse LysoIP sample including those derived from
97 *Grn* WT mice. This is in line with progranulin being primarily expressed in neurons and microglia
98 [29]. Protein concentrations were normalized prior to tandem mass tag mass spectrometry (TMT-
99 MS). Splenic macrophage-derived lysosomes were also obtained from *Cx3cr1-Cre* mice to further
100 characterize the effect of progranulin loss on immune cell lysosomes. Western blot verification
101 demonstrated reliable and specific isolation of lysosomes from all four Cre lines (Figure 1b-e).
102 Interestingly, in *Cx3cr1-Cre* LysoIP samples, Lamp1, a marker for lysosomal membranes,
103 demonstrated a molecular weight shift from ~75 kDa to ~110 kDa (Figure 1c). This was seen in
104 both whole-cell lysate and LysoIP samples from mouse spleens – an organ primarily comprised
105 of immune cells (Supplemental Figure 1a), suggesting this shift is specific to immune cells and is
106 thus unlikely to be seen in whole-brain lysates. Lamp1 has various glycosylation sites which likely
107 lead to this mass shift [30].

108 After TMT-MS, raw protein intensities were processed and normalized as described in
109 Methods (Supplemental Figure 1b-e). Several thousand proteins were detected in each TMT-MS
110 run (*Ubc-Cre*: 2310 proteins, *Cx3cr1-Cre* (Brain): 2302 proteins, *Cx3cr1-Cre* (Spleen): 1972
111 proteins, *Aldh1l1-Cre*: 2263 proteins, and *Syn-Cre*: 2219 proteins). To ensure stringent analysis
112 of the lysosomal proteome only, LysoIP samples were compared to no *Cre* control samples added
113 to each TMT-MS run (Figure 1f-i, Supplemental Figure 1f), and proteins were only included for
114 further analysis if they were significantly enriched in LysoIP samples compared to no *Cre* controls
115 and if their normalized abundance was at least 1.5x that of no *Cre* controls. This resulted in
116 hundreds of proteins per *Cre* line (*Ubc-Cre*: 332 proteins, *Cx3cr1-Cre* (Brain): 111 proteins,
117 *Cx3cr1-Cre* (Spleen): 147 proteins, *Aldh1l1-Cre*: 285 proteins, and *Syn-Cre*: 295 proteins). Gene

118 ontology analysis of the resultant proteins demonstrated significant enrichment for lysosomal
119 compartments (Figure 1j-m).

120 Between all TMT-MS runs, 526 unique lysosomal proteins were detected in both *Grn* WT
121 and *Grn* KO LysoIP samples. Several of these proteins were shared between at least 2 individual
122 Cre lines; however, 45.4% of all proteins detected were only detected in a single Cre line (Figure
123 1f). This most likely represents a cell type-specific lysosomal proteomic landscape [28]. These
124 proteins were then compared between *Grn* WT, *Grn* heterozygous, and *Grn* KO LysoIP samples
125 of the same Cre using ANOVA and multiple comparison correction as outlined in Methods. Any
126 protein with an adjusted p-value < 0.05 was considered significant. Comparing significantly
127 altered proteins between Cre lines, most significantly altered proteins were detected in neuronal
128 lysosomes (*Syn-Cre*) (Figure 1o, j). When comparing the number of significantly altered proteins
129 in individual Cre lines to the total number of proteins detected, microglial and neuronal lysosomes
130 demonstrated the highest percentage of significantly altered proteins (26.1% and 40.0%,
131 respectively) (Supplemental Figure 1h-k). This is consistent with progranulin primarily being
132 expressed in microglia and neurons. Gene ontology analysis of all significantly altered lysosomal
133 proteins across Cre lines – using all 526 lysosomal proteins as background – highlights
134 carbohydrate derivative catabolism, lipid storage, lysosomal organization, glycoprotein
135 catabolism, and cholesterol efflux as some of the most highly enriched cellular processes affected
136 by progranulin deficiency (Figure 1p; Supplemental Table 1).

137

138 <u>Changes to progranulin-deficient lysosomes are not reflected in mRNA or whole-cell lysate</u>
139 <u>changes</u>

140 Comparing *Ubc-Cre+ Grn* WT and *Grn* KO samples, progranulin deficiency significantly
141 altered 13/332 proteins with 8 of these proteins being upregulated and 5 downregulated (Figure
142 2a-c; Supplemental Table 2) while lysosomes from *Grn* heterozygous mouse brains did not
143 demonstrate any significant changes (Figure 2b). Proteins associated with endo-lysosomal

144 trafficking such as Tspan7 were significantly upregulated in *Grn* KO *Ubc-Cre* LysoIP samples [31,
145 32]. Tspan 7 has also been associated with synaptic transmission [33, 34]. Interestingly, Tthy2
146 and Ttyh3 are also significantly upregulated in *Grn* KO *Ubc-Cre* LysoIP samples. Tthy2 was
147 recently shown to interact with ApoE and facilitate endosomal lipid transfer [35]. The APOE4 allele
148 is the strongest genetic predictor for Alzheimer's disease (AD), and patients with GRN mutations
149 are also genetically predisposed to AD, suggesting the effect of progranulin deficiency on
150 lysosomal Tthy2 may contribute to this increased risk of developing AD [36, 37].

151 We next compared progranulin-deficient LysoIP samples against TMT-MS results of
152 progranulin-deficient whole brain lysates (Figure 2d-e) [38]. 237 proteins were shared between
153 these datasets; however, only progranulin was found to be significantly altered in both LysoIP and
154 whole brain samples. There was overall poor correlation between progranulin-dependent changes
155 from these datasets, suggesting the effects of progranulin deficiency on the lysosomal proteome
156 can primarily only be detected by directly measuring lysosomal proteins as previously reported
157 [39]. Further, comparisons between $\log_2$FC's of the 301 proteins detected in both our *Grn* KO
158 LysoIP samples and *Grn* KO RNA-Seq datasets from Evers *et al.* 2017 similarly demonstrate lack
159 of overlap in significantly altered proteins (Figure 2f) [13], and when comparing all proteins
160 detected in *Ubc-Cre* LysoIP samples to their respective mRNA transcripts from whole-brain RNA-
161 Seq data, no significant correlation can is detected (Figure 2g). This implies progranulin deficiency
162 alters the lysosomal proteome at the post-transcriptional level.

163

164 <u>Progranulin deficiency causes minor changes in astrocyte lysosomes</u>

165 Progranulin expression in astrocytes is relatively low compared to other cell types in the
166 brain [29]. In fact, TMT-MS analysis of 3-month-old *Aldh1l1-Cre* LysoIP samples did not detect
167 progranulin. However, progranulin was detected in 6-month-old *Aldh1l1-Cre* LysoIP samples, and
168 comparisons of these samples demonstrated 15/285 significantly altered lysosomal proteins
169 between *Grn* WT vs *Grn* KO mouse brains, with 3 being significantly upregulated and 12 being

170 significantly downregulated (Figure 2h-i, Supplemental Table 3). Similar to *Ubc-Cre* experiments,
171 the membrane protein Ttyh2 is upregulated in *Grn* KO astrocyte lysosomes, and several proteins
172 involved in sphingolipid metabolism such as Galc and Gba1 are downregulated [40, 41]. Galc and
173 Gba1 mutations have also both been implicated in Parkinsons disease [42, 43].
174
175 Progranulin deficiency dysregulates various disease-related proteins in the neuronal lysosome
176 In contrast to the minimal effect of progranulin loss on *Ubc-Cre*+ and *Aldh1l1-Cre*+ LysoIP
177 samples, progranulin deficiency heavily influences the neuronal lysosomal proteome, leading to
178 118/295 proteins being significantly altered with 59 proteins being upregulated and 59 being
179 downregulated (Figure 3a-b; Supplemental Table 4). PCA demonstrates clear delineation
180 between *Grn* WT and *Grn* KO neuronal lysosomes while *Grn* heterozygous lysosomes are more
181 heterogeneous between samples (Figure 3c). When investigating the cellular functions related to
182 significantly altered proteins in *Grn* KO neuronal lysosomes, gene ontology analysis demonstrates
183 sphingolipid biosynthesis, lipid biosynthesis, and lysosome organization as the most highly
184 enriched terms (Figure 3d; Supplemental Table 5). Proteins associated with ceramide metabolism
185 such as Neu4, Asah1, Asah2, and Gba1 are all downregulated in *Grn* KO neuronal lysosomes
186 (Figure 3e). Key autophagy proteins that are part of mTORC1 including mTor, Mlst8, and Rptor
187 are all significantly upregulated in *Grn* KO neuronal lysosomes while the adaptor proteins
188 Lamtor2, Lamtor4, and the amino acid transporter Slc38a9 are all significantly downregulated
189 [44]. This dysregulation may contribute to the impaired autophagy previously described in models
190 of progranulin deficiency [45, 46].
191 Several mitochondrial proteins including Vdac1/2/3 and Samm50 are all upregulated in
192 *Grn* KO neuronal lysosomes (Supplemental Figure 2a) [47-50]. Progranulin deficiency has been
193 implicated in mitophagy defects [51, 52], so we performed Seahorse analysis to determine if
194 mitochondria in *Grn* KO mouse brains demonstrated decreased function. We did not observe any
195 overt mitochondrial deficits using this method (Supplemental Figure 2b-c). However, we did detect

196 a significantly decreased NAD+/NADH ratio from *Grn* KO mouse brains compared to *Grn* WT
197 (Supplemental Figure 2d-f). This was driven by both an increase in NADH and a decrease in
198 NAD+ in *Grn* KO mouse brains and demonstrates how progranulin deficiency alters brain energy
199 homeostasis.

200 Mfsd8 was the most significantly downregulated protein between *Grn* WT and *Grn* KO
201 LysoIP samples. Homozygous MFSD8 nonsense mutations lead to a classic lysosomal storage
202 disorder (CLN7), and missense mutations have also been found to be associated with FTD in a
203 small subset of patients [53]. Western blot analysis verified Mfsd8 was heavily decreased in *Grn*
204 KO neuronal lysosomes (Figure 3f-g). Mfsd8 was not detected in either astrocyte or microglial
205 LysoIP samples, suggesting it is specific to neuronal lysosomes and thus only regulated by
206 neuronal progranulin.

207 Of the proteins significantly dysregulated in *Grn* KO neuronal lysosomes, 32 of them are
208 known lysosomal proteins associated with known neurologic disorders based on the OMIM
209 database (Figure 3h, Table 1) [28]. This includes proteins associated with lysosomal storage
210 disorders such as Mfsd8, Smpd1, Galc, and Asah1 [40, 54-56].

211

212 <u>Progranulin deficiency dysregulates disease-relevant proteins in the microglial lysosome</u>

213 While fewer total lysosomal proteins were detected in *Cx3cr1-Cre* LysoIP samples – likely
214 due to less starting material – several key lysosomal proteins were found to be dysregulated
215 secondary to progranulin deficiency with a total of 29/111 proteins being significantly altered with
216 14 proteins being upregulated and 15 being downregulated (Figure 4a-c; Supplemental Table 6).
217 Based on GO analysis, progranulin deficiency in microglia primarily affects lysosomal proteins
218 associated with lipid catabolism and tissue regeneration, both processes known to be
219 dysregulated in models of progranulin deficiency [13, 57] (Figure 4d; Supplemental Table 7).

220 To test whether the effects of progranulin deficiency on lysosomal protein composition
221 were specific to microglia or were universal to all immune cells, we performed TMT-MS analysis

222 on LysoIP samples derived from spleens of *Cx3cr1-Cre*+; *Grn* WT and KO mice. This analysis
223 revealed several proteins significantly altered in *Grn* KO splenic macrophage lysosomes
224 compared to *Grn* WT (Supplemental Figure 3a-c; Supplemental Table 8). However, when
225 comparing proteins between *Grn* KO microglial and splenic macrophages by principal component
226 analysis, the two tissue types clustered separately (Figure 4e) and several proteins were found
227 to be significantly different (Figure 4f). This suggests the effects of progranulin deficiency on
228 immune cells are in part dependent on the tissue of origin. Of note, Pld4 is significantly
229 downregulated in progranulin deficient microglia (log_2FC = -1.00, adjusted p-value = 0.003). Pld4
230 was recently discovered to be a synthetic protein for BMPs within the lysosomes of immune cells
231 [58]. BMPs are also significantly downregulated in models of progranulin deficiency and are key
232 lysosomal lipids that act as mediators of catabolic processes [12, 14]. These data suggest loss of
233 BMPs in progranulin deficient brains may be in part secondary to progranulin-dependent Pld4
234 deficiency.

235 We were also interested to test whether the changes we saw in the microglial lysosomal
236 proteome were reflected in microglial RNA-Seq data. To accomplish this, we compared the
237 log2FC's of *Cx3cr1-Cre*+;*Grn* KO LysoIP samples to *Grn* KO mRNA samples from a previously
238 published microglial RNA-Seq datasets (Figure 4g) [59]. 80 of the 111 LysoIP proteins were
239 detected in the RNA-Seq dataset. This included 18 proteins that are significantly altered in the
240 *Cx3cr1-Cre* LysoIP dataset. However, the log2FC values of these proteins did not correlate to the
241 log2FC values of their accompanying transcripts (r^2 = 0.029). This suggests the majority of the
242 effects of progranulin deficiency on the microglial lysosomal proteome are not secondary to
243 alterations at the mRNA level.

244 One of the proteins most significantly downregulated in *Grn* KO microglial lysosomes is
245 palmitoyl protein thioesterase 1 (Ppt1). Mutation of this protein leads to neuronal ceroid
246 lipofuscinosis 1 (CLN1), an early onset lysosomal storage disorder with severe symptoms such
247 as microcephaly, hypotonia, and epilepsy [60]. Western blot analysis of LysoIP samples from

248 brains of *Cx3cr1-Cre*+, *Syn-Cre*+, and *Ubc-Cre*+ mice demonstrates Ppt1 is effectively absent
249 from microglial lysosomes but not significantly altered in whole-brain or neuronal lysosomes
250 (Figure 4h-k). In our TMT-MS datasets, Ppt1 is significantly down-regulated in *Syn-Cre*+;*Grn* KO
251 LysoIP samples compared to *Grn* WT controls, and while Western blot analysis of these samples
252 does not recapitulate these findings, there is certainly a trend for decreased Ppt1 in *Grn* KO
253 neuronal lysosomes. Regardless, the effect of progranulin deficiency on microglial Ppt1 is much
254 larger than the effect on neuronal Ppt1 in both TMT-MS and western blot analysis.

255 While Ppt1 is absent in *Grn* KO microglial lysosomes, it is plausible progranulin deficiency
256 leads to accumulation of Ppt1 in non-lysosomal compartments. To test this possibility, we isolated
257 microglia and microglial lysosomes from the left and right hemibrains of 9 to 12-month-old *Cx3cr1-*
258 *Cre*+ mice, respectively (see Methods). Western blot analysis of both whole microglial and
259 microglial lysosome samples demonstrated significantly decreased levels of Ppt1 in *Grn* KO mice
260 compared to *Grn* WT (Figure 5l-n). This decrease was not significantly different between whole
261 microglia and microglial lysosomes, suggesting progranulin deficiency does not lead to
262 accumulation of missorted lysosomal proteins but instead causes overall decreases of microglial
263 lysosomal proteins.

264 Progranulin deficiency has also been associated with hyperinflammatory states [24, 61,
265 62]. Further, mutations in several other CLN-related proteins – including Ppt1 – have been shown
266 to increase the activation of the cGAS-STING pathway [63, 64]. Ppt1 has also been shown to
267 remove the palmitoyl moiety from phosphorylated STING in order to abrogate STING activation
268 [65]. To determine if progranulin deficiency led to increased STING signaling similar to other CLN
269 genes, we produced *GRN* KO HeLa cells and measured phosphorylated STING as a function of
270 time after activation with the STING agonist diABZI [66]. In the presence of prolonged STING
271 activation, p-STING is known to peak and decline as it becomes digested by the lysosome [67].
272 However, in *GRN* KO cells, STING activation (measured by p-STING levels) was significantly
273 prolonged (Supplemental Figure 4a-d). This suggests progranulin deficiency leads to

274 hyperinflammation in part through prolonged activation of the STING pathway potentially caused
275 by decreased Ppt1-mediated pSTING depalmitoylation. Overall, our data indicate progranulin
276 deficiency impairs microglial lysosomal homeostasis leading to a secondary hyperinflammatory
277 state.
278
279 **Discussion**
280 Progranulin deficiency has long been known to affect lysosomal function with loss of
281 progranulin leading to impaired lysosomal size and shape, impaired lysosomal lipid composition,
282 impaired lysosomal pH regulation, and impaired lysosomal protein activity [10, 12-15]. Previous
283 work by our lab and others has further shown that progranulin deficiency leads to aberrations of
284 the lysosomal proteome [16, 17, 68]. However, the effect of progranulin deficiency on lysosomal
285 composition in the mammalian brain has not been studied in a cell type-dependent manner. To
286 this end, we utilized an immunoprecipitation-based system to isolate lysosomes from specific cell
287 types in *Grn* WT, heterozygous, and KO mouse brains and spleens. TMT-MS analysis of these
288 samples demonstrated that neuronal and microglial lysosomes were most affected by progranulin
289 deficiency; however, progranulin deficiency led to diverging effects between these cell types.
290 When comparing *Grn* KO LysoIP samples, PCA demonstrates clear separation between
291 lysosomes of different cell types (Figure 5a, Supplemental Table 9). Further analysis
292 demonstrates several proteins whose $\log_2$FC's between *Grn* WT and *Grn* KO are significantly
293 different between *Cx3cr1-Cre+* and *Aldh1l1-Cre+*, *Aldh1l1-Cre+* and *Syn-Cre+*, and *Cx3cr1-Cre+*
294 and *Syn-Cre+* (Figure 5b-d. Supplemental Table 10) LysoIP samples.
295 Progranulin deficiency leads to some proteins such as Naaa and Arsg being significantly
296 downregulated in one cell type and unchanged or even upregulated in another; however,
297 comparisons of proteins significantly altered between *Grn* WT and *Grn* KO LysoIP samples in at
298 least one Cre line demonstrate overall trends of most proteins being consistently up- or
299 downregulated between cell types (Figure 5e-f). Despite this, most proteins affected by

300 progranulin deficiency exhibit cell type-specific sensitivities to this deficiency. For instance, Ppt1,
301 while downregulated between *Grn* WT and *Grn* KO LysoIP samples in all cell types, is more
302 downregulated in microglia compared to astrocytes or neurons. In line with these findings, we
303 propose a hypothetical model where certain proteins are either entirely dependent, somewhat
304 dependent, or independent on progranulin for proper localization and/or stability within the
305 lysosome in a cell type-dependent manner (Figure 6). This model is supported by progranulin
306 being found to physically interact with secretory proteins such as the inflammatory mediator
307 sPLA2-IIa as well as the lysosomal proteins Ctsd, Smpd1, and Gba1, the latter two of which are
308 down-regulated in progranulin deficient lysosomes within the mouse brain [11, 69-71]. Of note,
309 these protein-protein interaction studies were performed at neutral pH, suggesting they could
310 occur in the less acidic ER or Golgi apparatus.

311 How progranulin affects the lysosomal proteome in a cell type-sensitive manner is not yet
312 understood; however, this could be achieved by composition-dependent multiprotein complex
313 formation or by certain cell types possessing unknown proteins whose functions are redundant to
314 progranulin, while other cell types are entirely dependent on progranulin for lysosomal localization
315 and/or stability of certain lysosomal proteins. This suggests progranulin may function similarly to
316 CLN6 and CLN8, which are responsible for promoting egress of lysosomal proteins from the ER-
317 Golgi complex, or to prosaposin, the precursor for the lysosomal enzyme activating saposins, an
318 established interaction partner for progranulin that is required in precise stoichiometric proportions
319 for efficient transport of progranulin to the lysosome [6, 72, 73].

320 Endo-lysosomal dysfunction has been implicated not just in GRN-FTD, but in several
321 neurodegenerative disorders such as Alzheimer's disease and Parkinson's disease as well [74].
322 As post-mitotic cells, neurons do not have the ability to dilute impaired lysosomes through cell
323 division. Lysosome membrane repair is also impaired in an age-dependent manner [75]. This
324 leads to accumulation of faulty lysosomes in older neurons, impairing proper macromolecule
325 degradation and nutrient signaling. Why some endo-lysosomal defects lead to the accumulation

326 of certain aggregate-prone proteins (e.g., alpha-synuclein, tau, TDP-43, etc.) is yet to be
327 understood, but the correlation between impaired lysosome function and neurodegeneration is
328 well established and may provide a therapeutic avenue for not just GRN-FTD, but for multiple
329 neurodegenerative disorders.

330 Currently, despite progranulin deficiency leading to 20% of familial FTD, there is no
331 approved treatment for GRN-FTD. Considering the vast network of lysosomal proteins affected
332 by progranulin deficiency in a cell-type sensitive manner, progranulin replacement at the protein
333 synthesis level, and not attempts to correct secondary consequences to lysosomal function or
334 composition, may be the best treatment strategy. Several potential treatments including protein
335 replacement, AAV-technologies, biologics, and small molecule inducers of progranulin expression
336 have emerged in both pre-clinical and clinical trials [14, 16, 76-79]. Pathological markers of
337 neurodegenerative diseases appear to accumulate well before the onset of symptoms [80-82],
338 and preventive treatment for these disorders, whenever possible, is likely to provide the best
339 protection against neurodegeneration. Because of its familial inheritance pattern, GRN-FTD is a
340 strong candidate for preventive treatment with progranulin-enhancing agents that aim at
341 increasing the expression of the full-length protein form the remaining functional allele to
342 normalize progranulin levels prior to disease onset. This treatment strategy could potentially stave
343 off the lysosomal aberrations seen in progranulin deficiency and even stall disease onset entirely.

344

345

346

347

348

349

350 **Figure Legends**

351 **Figure 1: *In vivo* LysoIP isolates cell-type-specific lysosomes from progranulin deficient**
352 **mice. a** Experimental design for cell-type-specific lysosomal isolation from progranulin deficient
353 mice followed by TMT-MS. **b-e** Western blot verification of *in vivo* LysoIP from all brain cells (*Ubc-*
354 *Cre*, **b**), microglia (*Cx3cr1-Cre*, **c**), astrocytes (*Aldh1l1-Cre*, **d**), and neurons (*Syn-Cre*, **e**). **f-i**
355 Volcano plots comparing LysoIP samples to no *Cre* controls (adjusted p-value < 0.05, one-sample
356 t-test followed by Benjamini-Hochberg correction). Known lysosomal proteins are marked as blue
357 triangles. **j-m** Gene ontology analysis of LysoIP samples from four separate *Cre* lines after
358 processing of raw TMT-MS peak intensities. **n** Venn diagram that demonstrates overlap of all
359 brain-derived, lysosomal proteins found in four separate *Cre* lines. **o** Venn diagram that
360 demonstrates overlap of significantly altered brain-derived, lysosomal proteins (*Grn* WT vs *Grn*
361 KO, adjusted p-value < 0.05) in four separate *Cre* lines. **p** Gene ontology analysis of significantly
362 altered, brain-derived lysosomal proteins found in all four *Cre* lines (*Grn* WT vs *Grn* KO, adjusted
363 p-value < 0.05).

364

365 **Figure 2. *In vivo* LysoIP analysis of 3-month-old *Ubc-Cre* mouse brains demonstrates post-**
366 **translational alterations in key lysosomal proteins. a** Volcano plot demonstrating significantly
367 altered proteins (*Grn* WT vs *Grn* KO adjusted p-value < 0.05) from whole-brain LysoIP TMT-MS
368 samples (n = 3 *Grn* WT, n = 3 *Grn* Het, n = 3 *Grn* KO). **b** Principal component analysis comparing
369 $\log_2$FC values between *Grn* WT, *Grn* Het, and *Grn* KO brain-derived, lysosomal proteins in *Ubc-*
370 *Cre* mice. **c** Heatmap demonstrating $\log_2$FC values for significantly altered, brain-derived
371 lysosomal proteins found in brain-derived *Ubc-Cre* LysoIP TMT-MS samples (*Grn* WT vs *Grn* KO,
372 adjusted p-value < 0.05). **d** Venn diagram of the overlap of significantly altered proteins (*Grn* WT
373 vs *Grn* KO, adjusted p-value < 0.05) between brain-derived *Ubc-Cre* LysoIP and previously
374 published whole brain, whole cell lysate TMT-MS experiments. **e** Venn diagram of the overlap of

375 significantly altered proteins/transcripts (*Grn* WT vs *Grn* KO, adjusted p-value/q-value < 0.05)
376 between brain-derived *Ubc-Cre* LysoIP TMT-MS samples and previously published whole brain
377 RNA-Seq data. **f** Comparison of all log_2FC values (*Grn* WT vs *Grn* KO) for proteins found in both
378 brain-derived *Ubc-Cre* LysoIP TMT-MS samples and previously published whole brain TMT-MS
379 datasets **g** Comparison of all log_2FC values (*Grn* WT vs *Grn* KO) for proteins/transcripts found in
380 both brain-derived *Ubc-Cre* LysoIP TMT-MS samples and previously published whole brain RNA-
381 Seq datasets. **h** Volcano plot demonstrating significantly altered proteins (*Grn* WT vs *Grn* KO
382 adjusted p-value < 0.05) from whole-brain *Aldh1l1-Cre* LysoIP TMT-MS samples (n = 5 *Grn* WT,
383 n = 5 *Grn* Het, n = 5 *Grn* KO). **i** Heatmap demonstrating log_2FC values for significantly altered,
384 brain-derived lysosomal proteins found in brain-derived *Aldh1l1-Cre* LysoIP TMT-MS samples
385 (*Grn* WT vs *Grn* KO, adjusted p-value < 0.05).

386 **Figure 3. *In vivo* LysoIP analysis of 3-month-old *Syn-Cre* mouse brains demonstrates**
387 **aberrations in disease-relevant lysosomal proteins in progranulin-deficient neurons. a**
388 Volcano plot demonstrating significantly altered proteins (*Grn* WT vs *Grn* KO adjusted p-value <
389 0.05) from neuronal LysoIP TMT-MS samples (n = 5 *Grn* WT, n = 5 *Grn* Het, n = 5 *Grn* KO). **b**
390 Heatmap demonstrating log_2FC values for significantly altered neuronal LysoIP samples (*Grn* WT
391 vs *Grn* KO, adjusted p-value < 0.05). **c** Principal component analysis comparing log_2FC values in
392 neuronal lysosomal proteins between *Grn* WT, *Grn* Het, and *Grn* KO mice. **d** Gene ontology
393 analysis of significantly altered neuronal lysosomal proteins (*Grn* WT vs *Grn* KO, adjusted p-value
394 < 0.05). **e** Significantly altered neuronal lysosomal proteins (*Grn* WT vs *Grn* KO, adjusted p-value
395 < 0.05) which are associated with sphingolipid metabolic processes based on gene ontology
396 analysis. **f-g** Western blot (**f**) and densitometry analysis (**g**) of Mfsd8 in neuronal lysosomes (n =
397 5 *Grn* WT, n = 4 *Grn* KO; ***p < 0.001, Students' t-test) **h** Significantly altered neuronal lysosomal
398 proteins (*Grn* WT vs *Grn* KO, adjusted p-value < 0.05) whose mutations are associated with
399 neurologic disease.

400

401 **Figure 4. *In vivo* LysoIP analysis of 3-month-old *Cx3cr1-Cre* mouse brains demonstrates**
402 **cell-specific loss of lysosomal storage disease-related protein in progranulin-deficient**
403 **microglia. a** Volcano plot demonstrating significantly altered proteins (*Grn* WT vs *Grn* KO
404 adjusted p-value < 0.05) from microglial LysoIP TMT-MS samples (n = 4 *Grn* WT, n = 7 *Grn* Het,
405 n = 6 *Grn* KO). **b** Gene ontology analysis of significantly altered microglial lysosomal proteins (*Grn*
406 WT vs *Grn* KO, adjusted p-value < 0.05). **c** Principal component analysis comparing $\log_2$FC
407 values in microglial lysosomal proteins between *Grn* WT, *Grn* Het, and *Grn* KO mice. **d** Heatmap
408 demonstrating $\log_2$FC values for significantly altered microglial LysoIP samples (*Grn* WT vs *Grn*
409 KO, adjusted p-value < 0.05). **e** Principal component analysis comparing $\log_2$FC (*Grn* WT vs *Grn*
410 KO) between brain- and spleen-derived *Cx3cr1-Cre* LysoIP samples. **f** Volcano plot
411 demonstrating significantly altered proteins (brain vs spleen adjusted p-value < 0.05) from brain-
412 and spleen-derived *Cx3cr1-Cre* LysoIP TMT-MS samples (n = 6 brain-derived, n = 6 spleen-
413 derived). **g** Comparison of log2FC values (*Grn* WT vs *Grn* KO) between *Cx3cr1-Cre* LysoIP
414 samples and microglial mRNA transcripts from a previously published RNA-Seq dataset. Red
415 circles indicate proteins significantly altered in *Cx3cr1-Cre*+;*Grn* KO LysoIP samples. **h-j** Western
416 blot analysis of Ppt1 in whole-brain (**h**) neuronal (**i**), and microglial (**j**) lysosomes derived from *Grn*
417 WT and KO mouse brains. **k** Densitometry analysis of Ppt1 protein in whole-brain, neuronal, and
418 microglial lysosomes derived from *Grn* WT and KO mouse brains. Values were standardized to
419 Lamp1 and normalized to *Grn* WT (whole-brain: n = 5 3-month-old *Grn* WT and n = 5 3-month-
420 old *Grn* KO; neuronal: n = 5 3-month-old *Grn* WT and n = 5 3-month-old *Grn* KO; microglia: n = 3
421 6-month-old *Grn* WT and n = 7 6-month-old *Grn* KO; ****p < 0.0001, Students' t-test). **l-m** Western
422 blot analysis of Ppt1 in microglial lysosomes (**l**) and whole microglia (**m**). Psd95, Eeat2, and Iba1
423 act as neuronal, astrocyte, and microglial markers, respectively. **n** Densitometry analysis of Ppt1
424 blots. Values were standardized to Lamp1 (**l**) or beta-actin (**m**) and normalized to *Grn* WT (n = 3

425 9-12-month-old *Grn* WT and n = 3 9-12-month-old *Grn* KO; **p < 0.01, two-way ANOVA with
426 Fisher's LSD test).

427

428 **Figure 5. *In vivo* LysoIP datasets demonstrate progranulin-dependent aberrations to the**
429 **lysosomal proteome are unique across brain cell types. a** Principal component analysis of
430 *Grn* KO LysoIP log_2FC values (*Grn* WT vs *Grn* KO) from four separate *Cre* lines. **b** Heatmap
431 depicting log_2FC values (*Grn* WT vs *Grn* KO) of all proteins detected as significantly altered in
432 *Grn* KO LysoIP samples (*Grn* WT vs *Grn* KO adjusted p-value < 0.05) in at least one *Cre* line. **c-**
433 **e** Volcano plots comparing log_2FC values of significantly altered proteins (*Grn* WT vs *Grn* KO
434 adjusted p-value < 0.05) between *Cx3cr1-Cre* and *Aldh1l1-Cre* (**c**), *Aldh1l1-Cre* and *Syn-Cre* (**d**),
435 and *Cx3cr1-Cre* vs *Syn-Cre* (**e**) *Grn* KO LysoIP samples. **f** Bar plot comparing log_2FC values (*Grn*
436 WT vs *Grn* KO) of key lysosomal proteins detected as significantly altered in *Grn* KO LysoIP
437 samples (*Grn* WT vs *Grn* KO adjusted p-value < 0.05) in at least one *Cre* line.

438

439 **Figure 6. Hypothetical model of how progranulin deficiency potentially alters the**
440 **lysosomal proteome in a cell-type specific way.** Hypothetical model depicting how in certain
441 cell-types, lysosomal proteins may be fully dependent, partially dependent, or independent of
442 progranulin for sorting to the lysosome. The variation between cell types may depend on yet
443 unknown cell-type specific redundant proteins that, like progranulin, also sort lysosomal proteins
444 to the lysosome. Some proteins, such as Mfsd8 in neurons or Ppt1 in microglia, are entirely or
445 nearly entirely dependent upon progranulin for their lysosomal delivery (left panels). Other
446 lysosomal proteins require progranulin for their efficient delivery, but can still complete their
447 journey there, albeit at reduced overall efficiency (middle panels). For other proteins, sorting to
448 the lysosome is undiminished even in the complete absence of progranulin (right panels).

449

450 **Supplemental Figure Legends**

451 **Supplemental Figure 1. TMT-MS analysis of LysoIP samples demonstrates progranulin-**
452 **dependent changes primarily in microglia and neurons. a-d** Violin plots of median-normalized
453 TMT-MS intensity measurements from *Ubc-Cre* (**a**), *Cx3cr1-Cre* (**b**), *Aldh1l1-Cre* (**c**), and *Syn-*
454 *Cre* (**d**) mice. Gm130 was used as a marker for Golgi apparatus, Lamp1 was used as a marker
455 for lysosomal membrane, calnexin was used as a marker for ER, Cathepsin B was used as a
456 marker for lysosomal lumen, and CoxIV was used as a marker for mitochondria. For *Cx3cr1-Cre*+
457 samples, cathepsin D was used as a marker for lysosomal lumen due to these samples being
458 imaged on Licor which was not compatible with our cathepsin B antibody. **e** Volcano plot
459 comparing spleen-derived *Cx3cr1-Cre* LysoIP samples to no *Cre* controls (adjusted p-value <
460 0.05, one-sample t-test followed by Benjamini-Hochberg correction). Known lysosomal proteins
461 are marked as blue triangles. **f** Gene ontology analysis of spleen-derived *Cx3cr1-Cre* LysoIP
462 samples after processing of raw TMT-MS peak intensities. **g** Lamp1 western blot of spleen- and
463 brain-derived *Cx3cr1-Cre* whole lysate, LysoIP, and no *Cre* control samples. **h-k** Pie charts
464 demonstrating percent of proteins significantly up- and down-regulated in whole-brain (**h**),
465 microglial (**i**), astrocyte (**j**), and neuronal (**k**) lysosomes.

466

467 **Supplemental Figure 2. Progranulin deficiency leads to aberrant mitochondrial protein**
468 **levels in neuronal lysosomes alongside energetic alterations. a** Log_2FC values of
469 mitochondrial proteins significantly increased in *Grn* KO neuronal lysosomes compared to *Grn*
470 WT (adjusted p-value < 0.05). **b-c** Seahorse analysis of electron flow (**b**) and electron coupling
471 (**c**) of isolated mitochondria from 15-month-old *Grn* WT and *Grn* KO mouse brains (n = 3 *Grn* WT
472 and n = 3 *Grn* KO; two-way ANOVA with multiple comparisons and Sidak correction). **d-f** Levels

473 of NADH (**d**), NAD+ (**e**), and NAD+/NADH ratios (**f**) from 15-month-old *Grn* WT, *Grn* Het, and *Grn*
474 KO mouse brains (n = 5 *Grn* WT, n = 4 *Grn* Het, n = 5 *Grn* KO; one-way ANOVA with multiple
475 comparisons and Dunnett correction, *p < 0.05, **p < 0.01, ***p < 0.0001).

476

477 **Supplemental Figure 3. *In vivo* LysoIP analysis of 3-month-old *Cx3cr1-Cre* mouse spleens**
478 **demonstrates progranulin-dependent changes in key lysosomal proteins. a** Volcano plot
479 demonstrating significantly altered proteins (*Grn* WT vs *Grn* KO, adjusted p-value < 0.05) from
480 splenic macrophage LysoIP TMT-MS samples (n = 6 *Grn* WT, n = 5 *Grn* Het, n = 5 *Grn* KO). **b**
481 Principal component analysis comparing $\log_2$FC values in splenic macrophage lysosomal proteins
482 between *Grn* WT, *Grn* Het, and *Grn* KO mice. **c** Venn diagram comparing significantly altered
483 proteins (*Grn* WT vs *Grn* KO, adjusted p-values < 0.05) in splenic macrophage and microglial
484 lysosomes.

485

486 **Supplemental Figure 4. Progranulin deficiency leads to altered STING dynamics *in vitro*. a**
487 Representative western blot of diABZI-mediated STING activation time course on *GRN* WT and
488 *GRN* KO HeLa cells. Beta-actin is used as a loading control. **b-d** Quantification of p-STING (**b**),
489 total STING (**c**), and phospho/total STING (**d**) of diABZI-mediated STING activation time course
490 (n = 4 *GRN* WT, n = 4 *GRN* KO; two-way ANOVA with multiple comparisons and Sidak correction,
491 *p < 0.05, **p < 0.01).

492

493 **Supplemental Tables**

494 **Supplemental Table 1:** Gene ontology analysis of LysoIP proteins significantly altered (*Grn* WT
495 vs *Grn* KO) in at least one Cre line

496 **Supplemental Table 2:** Log_2FC and p-values for TMT-MS data for individual mouse LysoIP data
497 from all *Ubc-Cre*+ lines compared to one another
498 **Supplemental Table 3:** Log_2FC and p-values for TMT-MS data for individual mouse LysoIP data
499 from all *Aldh1l1-Cre*+ lines compared to one another
500 **Supplemental Table 4:** Log_2FC and p-values for TMT-MS data for individual mouse LysoIP data
501 from all *Syn-Cre*+ lines compared to one another
502 **Supplemental Table 5:** Gene ontology analysis of LysoIP proteins significantly altered (*Grn* WT
503 vs *Grn* KO) in *Syn-Cre*+;*Grn* KO LysoIP samples
504 **Supplemental Table 6:** Log_2FC and p-values for TMT-MS data for individual mouse, brain
505 derived LysoIP data from all *Cx3cr1-Cre*+ lines compared to one another
506 **Supplemental Table 7:** Gene ontology analysis of brain-derived LysoIP proteins significantly
507 altered (*Grn* WT vs *Grn* KO) in *Cx3cr1-Cre*+;*Grn* KO LysoIP samples
508 **Supplemental Table 8:** Log_2FC and p-values for TMT-MS data for individual mouse, spleen
509 derived LysoIP data from all *Cx3cr1-Cre*+ lines compared to one another
510 **Supplemental Table 9:** Log_2FC and p-values for TMT-MS data for individual mouse, brain-
511 derived LysoIP data from all all Cre lines
512 **Supplemental Table 10:** Log_2FC and p-values for TMT-MS data for individual mouse, brain-
513 derived LysoIP data comparing log_2FC (vs *Grn* WT) values of *Grn* KO samples between Cre
514 lines

515 **Materials used in the study**

REAGENT or RESOURCE	SOURCE	IDENTIFIER
Antibodies		
Mouse anti-Golgin 97	Santa Cruz	Cat #: sc-73619
Rat anti-Lamp1	DSHB	Clone 1D4B
Rabbit anti-Calreticulin	Cell Signaling	Cat #: 12238
Rabbit anti-Cathepsin B	Cell Signaling	Cat #: 31718
Rabbit anti-CoxIV	Cell Signaling	Cat #: 4850
Rabbit anti-Gm130	Invitrogen	Cat #: MA5-35107
Rabbit anti-Calnexin	Enzo	Cat #: ADI-SPA-860
Rabbit anti-Cathepsin D	Abcam	Cat #: ab75852
Rabbit anti-Mfsd8 (Cln7)	Proteintech	Cat #: 24298-1-AP
Rabbit anti-Progranulin	Sigma	Cat #: HPA008763
Rabbit anti-Ppt1 (Cln1)	Proteintech	Cat #: 29653-1-AP
Rabbit anti-Psd95	Cell Signaling	Cat #: 2507
Rabbit anti-Eaat2	Abcam	Cat #: ab41621
Rabbit anti-Iba1	Wako FujiFilm	Cat #: 019-19741
Rabbit anti-beta-Actin	Abcam	Cat #: ab8227
Rabbit anti-Sting	Cell Signaling	Cat #: 13647
Rabbit anti-phospho-STING (S366)	Cell Signaling	Cat #: 19781
Bacterial and virus strains		
pX330-U6-Chimeric_BB-CBh-hSpCas9	Addgene	Plasmid #: 42230

Biological samples		
Chemicals, peptides, and recombinant proteins		
Lipofectamine	Thermo Scientific	Cat #: 11668030
diabzi-Sting-Agonist-3-(Hydrochloride)	Cayman Chemical	Cat #: 28054-NC2223805
Rotenone	Sigma	Cat #: 557368
Sodium Succinate	Sigma	Cat #: S2378
Antimycin A	Thermo Scientific	Cat #: J63522.MA
Sodium Ascorbate	Sigma	Cat #: PHR1279
TMPD	Sigma	Cat #: T7394
ADP	Sigma	Cat #: 01905
Oligomycin	Sigma	Cat #: O4876
FCCP	Sigma	Cat #: C2920
Trypsin	Thermo Scientific	Cat #: 90056
Critical commercial assays		
MicroBCA Protein Assay Kit	Thermo Scientific	Cat #: 23235
NAD/NADH Assay Kit	Abcam	Cat #: ab65348

Deposited data		
Mass spectrometry proteomics data (Grn WT vs Het vs KO LysoIP raw data)	This paper	MassIVE: Dataset accession number: MSV000099828 Password: UTSW2025 ftp://MSV000099828@massive-ftp.ucsd.edu
Raw western blot and downstream proteomics analysis	This paper	Texas Data Repository
Bulk RNA-Seq data (Grn WT vs KO)	Evers et al.[13]	DOI: 10.1016/j.celrep.2017.08.056
Whole Brain TMT-MS (Grn WT vs KO)	Huang et al.[40]	DOI: 10.1186/s40478-020-01037-x

Microglial RNA-Seq (Grn WT vs KO)	Zhang et al.[56]	DOI: 10.1007/s00401-023-02578-w
Experimental models: Cell lines		
HeLa (WT)	ATCC	Cat #: CCL-2
HeLa Grn KO	This paper	N/A
Experimental models: Organisms/strains		
C57BL/6 (Grn WT, Het, KO)	Evers et al.[13]	N/A
B6.129S4-Gt(ROSA)26Sortm1(CAG-TMEM192)Dmsa/J	Jackson Labs	Strain #: 035401
B6.Cg-Ndor1Tg(UBC-cre/ERT2)1Ejb/2J	Jackson Labs	Strain #: 008085
B6.Cg-Tg(Syn1-cre)671Jxm/J	Jackson Labs	Strain #: 003966
B6.129P2(C)-Cx3cr1tm2.1(cre/ERT2)Jung/J	Jackson Labs	Strain #: 020940
B6;FVB-Tg(Aldh1l1-cre/ERT2)1Khakh/J	Jackson Labs	Strain #: 029655
Oligonucleotides		
Grn KO gRNA: 5'-GGATCGAGCCTTCACGTTGCAGG-3'	This paper	N/A
Primer: Grn WT For 5'-agtggggctggccacttct-3′	Evers et al.[13]	N/A
Primer: Grn Mut For 5'-aagattcctcgctgggacatg-3′	Evers et al.[13]	N/A
Primer: Grn WT/Mut Rev 5'-gaatgctggtgtcagagggcc-3′	Evers et al.[13]	N/A

Primer: TMEM192-3xHA wt/wt For 5'-CTGGCTTCTGAGGACCG-3'	Laqtom et al.[27]	N/A
Primer: TMEM192-3xHA wt/wt Rev 5'-AATCTGTGGGAAGTCTTGTCC-3'	Laqtom et al.[27]	N/A
Primer: TMEM192-3xHA fl/fl For 5'-TCCTTGGATATCACCCAGAGT-3'	Laqtom et al.[27]	N/A
Primer: TMEM192-3xHA fl/fl Rev 5'-CCACAAAATAACTTTCCCAAGG-3'	Laqtom et al.[27]	N/A
Primer: UBC-/Syn-/Aldh1l1-Cre For 5'-GCTGCCACGACCAAGTGACAGCAATG-3'	This paper	N/A
Primer: UBC-/Syn-/Aldh1l1-Cre Rev 5'-GTAGTTATTCGGATCATCAGCTACAC-3'	This paper	N/A
Primer: Cx3cr1-Cre WT For 5'-GTGGGAAATCTGTTGGTGGTCCTC-3'	This paper	N/A
Primer: Cx3cr1-Cre Mut For 5'-GTTAATGACCTGCAGCCAAG-3'	This paper	N/A
Primer: Cx3cr1-Cre WT/Mut Rev 5'-TAGTCACCCAGACACTCGTTGTCC-3'	This paper	N/A
Recombinant DNA		
Software and algorithms		

Prism	GraphPad	https://www.graphpad.com/features
ImageJ	Schneider et al.	https://imagej.net/ij/
RStudio	Posit Team (2024)	http://www.posit.co/
Limma	Ritchie et al.[89]	DOI: 10.18129/B9.bioc.limma
Other		
Anti-HA Dynabeads	Thermo Scientific	Cat # 88836
Anti-Cd11b MicroBeads	Miltenyi Biotec	Cat #: 130-093-636

516

517 **Methods**

518 Cell Culture

519 All cell culture reagents and plates were purchased from Corning (Corning, NY, USA). Cells were
520 maintained at 8.8% CO2 at 37 °C. HeLa cells were cultured in high glucose Dulbecco's Modified
521 Eagle's Medium (DMEM) with 10% FCS and Pen/Strep and supplied from ATCC (CCL-2).

522

523 Generation of *GRN* KO HeLa cells

524 HeLa cells were transfected with a plasmid containing both Cas9 and sgRNA targeting the R493
525 region of progranulin as this is one of the most commonly mutated residues [83]. Transfection
526 was performed with Lipofectamine 2000 in a ratio of 6:1 (6 μL Lipofectamine: 1 μg DNA). 48-72
527 hours after transfection, positive cells were selected using puromycin, and individual clones were
528 isolated, grown, and tested for progranulin via western blot.
529
530 STING activation assay
531 HeLa cells were grown in 6-well plates to 80-90% confluence and were treated with 1 μM diABZI
532 added to 1 mL fresh media for 0, 1, 2, 4, 8, or 12 hours at 37°C. At designated timepoints, cells
533 were rinsed three times with cold PBS on ice, and protein was harvested by scraping cells in 100
534 μL lysis buffer. Cells were incubated with lysis buffer for 15 minutes at 4°C, insoluble material was
535 pelleted by centrifugation at 21,130g for 10 minutes at 4°C, and supernatant was moved to fresh
536 tube. STING activation was measured by western blot analysis using antibodies to human
537 phospho-STING (Ser 366) and total STING.
538
539 Generation of Grn;TMEM192-3xHA fl/fl mice and animal husbandry
540 The *Grn* mutant mice were originally obtained from the Farese lab and were propagated for at
541 least 50 generations in the Herz lab. Their generation is previously described [13]. Animals were
542 maintained on a C57BL/6 J background by heterozygous intercrossing. *Grn* KO mice were bred
543 with TMEM192-3xHA fl/fl mice obtained from Jackson Labs (Strain #035401) [27]. *Grn*
544 KO;TMEM192-HA fl/fl mice were then crossbred with either *Ubc-Cre*^{ERT2} (Jackson Labs Strain
545 #008085), *Syn-Cre* (Jackson Lab Strain #003966), *Cx3cr1-Cre*^{ERT2} (Jackson Labs Strain
546 #020940), or *Aldh1l1-Cre*^{ERT2} (Jackson Labs Strain #029655) mice to establish *Grn* WT,
547 heterozygous, or KO; TMEM192-3xHA fl/fl; Cre+ mice. To induce expression of UBC-, Cx3cr1-,
548 and Aldh1l1-Cre, animals were injected at 8 weeks with tamoxifen (120 mg/kg) for up to 5 days.

549 Animals were maintained on a 12 h light/12-h dark cycle and fed a standard rodent chow diet (Diet
550 7001; Harlan Teklad, Madison, WI) and water ad libitum. No sexual dimorphism of phenotype was
551 observed, and both male and female mice were used for all experiments. All procedures were
552 performed in accordance with the protocols approved by the Institutional Animal Care and Use
553 Committee of the University of Texas Southwestern Medical Center (IACUC APN 2015-101088-
554 G).
555
556 *In vivo LysoIP*
557 For isolation of lysosomes from mouse brain, a similar protocol was used as previously described
558 [27, 28]. Each LysoIP was individually completed before the next LysoIP was performed. 2-3-
559 month-old (for *Ubc-Cre*, *Cx3cr1-Cre*, and *Syn-Cre*) or 6-month-old (for *Aldh1l1-Cre*) mice were
560 anesthetized with isoflurane and immediately perfused with ice cold PBS (5 mL administered over
561 4-5 minutes). The brain was removed from the skull, and the olfactory bulbs were removed. Brains
562 were cut into 6 pieces and placed in 950 μL homogenization buffer (PBS + protease inhibitor +
563 phosphatase inhibitor). Brains were homogenized on ice with 25 strokes of plunger, and
564 homogenate was moved to 2 mL microcentrifuge tube. 25 μL of homogenate was moved to
565 separate tube for whole cell lysate. 1 mL of homogenization buffer was added to homogenate to
566 decrease pipetting errors. Insoluble material was spun down at 1000g for 2 min at 4°C. All further
567 steps were performed at 4°C.
568
569 1 mL homogenate was added to 100 μL anti-HA Dynabeads which had been pre-washed in 1 mL
570 cold PBS three times before experiment. Homogenate was incubated with Dynabeads with end-
571 over-end rotation for 15 minutes. After incubation, supernatant was removed from Dynabeads,
572 and Dynabeads were washed with 1 mL homogenization buffer three times. After the third wash,

573 Dynabeads were moved to fresh tube. 180 μL lysis buffer was added to Dynabeads and incubated
574 on ice for 15 minutes. Lysis buffer was removed from Dynabeads and moved into fresh tube.
575 For LysoIP of splenic macrophages, the same procedure was used as for the brain, except mice
576 were not perfused with PBS before dissection of the spleen, and 300 μL homogenization buffer
577 was added to homogenate (as opposed to 1 mL with brain LysoIP). All remaining steps were the
578 same as for brain LysoIP.
579
580 For whole cell lysate, 200 uL lysis buffer was added to lysate and incubated with end-over-end
581 rotation for 15 minutes. Insoluble material was spun down at 21,130g for 10 min at 4°C. Lysate
582 was moved to fresh tube, and both lysate and LysoIP were stored at -80°C until downstream
583 applications.
584
585 Tandem mass tag mass spectrometry
586 Sample concentrations were measured by micro-BCA assay and normalized to sample with
587 lowest concentration. Samples were dried for 30 min in a SpeedVac, after which 40 µl of 5% SDS
588 was added to each. Samples were then reduced with TCEP and alkylated with iodoacetamide in
589 the dark. Each sample was loaded onto an S-Trap Micro (Protifi), following which 2 µg of trypsin
590 (Pierce) was added and allowed to digest overnight at 37 °C. Peptides were eluted and dried in a
591 SpeedVac, then were reconstituted in 21 µl of 50 mM TEAB buffer. Samples were then each
592 labeled with 4 µl of TMTpro 16plex reagent (ThermoFisher, Waltham, MA, USA, A44520) and
593 quenched with 2 µl of 5% hydroxylamine and combined in equal peptide amount based on
594 NanoDrop A205 reading. These mixtures were dried in a SpeedVac and reconstituted in 2%
595 acetonitrile, 0.1% TFA buffer.
596

597 Peptides were analyzed on a Thermo Orbitrap Eclipse MS system coupled to an Ultimate 3000
598 RSLC-Nano liquid chromatography system. Samples were injected onto a 75 um i.d., 75-cm long
599 EasySpray column (Thermo) and eluted with a gradient from 0-28% buffer B over 180 min at a
600 flow rate of 250 nL/min. Buffer A contained 2% (v/v) ACN and 0.1% formic acid in water, and buffer
601 B contained 80% (v/v) ACN, 10% (v/v) trifluoroethanol, and 0.1% formic acid in water. at a flow
602 rate of 250 nl/min. Spectra were continuously acquired in a data-dependent manner throughout
603 the gradient, acquiring a full scan in the Orbitrap (at 120,000 resolution with a standard AGC
604 target) followed by MS/MS scans on the most abundant ions in 2.5 s in the ion trap (turbo scan
605 type with an intensity threshold of 5,000, CID collision energy of 35%, standard AGC target,
606 maximum injection time of 35 ms and isolation width of 0.7 m/z). Charge states from 2-6 were
607 included. Dynamic exclusion was enabled with a repeat count of 1, an exclusion duration of 25 s
608 and an exclusion mass width of ± 10 ppm. Real-time search was used for selection of peaks for
609 SPS-MS3 analysis, with searched performed against a list of proteins from the mouse reviewed
610 protein database from UniProt. Up to 2 missed tryptic cleavage was allowed, with
611 carbamidomethylation (+57.0215) of cysteine and TMTpro reagent (+304.2071) of lysine and
612 peptide N-termini used as static modifications and oxidation (+15.9949) of methionine used as a
613 variable modification. MS3 data were collected for up to 10 MS2 peaks which matched to
614 fragments from the real-time peptide search identification, in the Orbitrap at a resolution of 50,000,
615 HCD collision energy of 65% and a scan range of 100–500.
616
617 Protein identification and quantification were done using Proteome Discoverer v.3.0 SP1
618 (Thermo). Raw MS data files were analyzed against the mouse reviewed protein database from
619 UniProt. Both Comet and SequestHT with INFERYS Rescoring were used, with
620 carbamidomethylation (+57.0215) of cysteine and TMTpro reagent (+304.2071) of lysine and
621 peptide N-termini used as static modifications and oxidation (+15.9949) of methionine used as a
622 variable modification. Reporter ion intensities were reported, with further normalization performed

623 by using the total intensity in each channel to correct discrepancies in sample amount in each
624 channel. A co-isolation threshold of 75% and an SPS Mass Matches threshold of 65% was used,
625 and the false-discovery rate (FDR) cutoff was 1% for all peptides.
626
627 Analysis of TMT-MS results
628 For each TMT-MS run, at least one sample from a Cre- mouse was included as a negative control.
629 All samples were normalized to total protein abundance. LysoIP samples were compared to the
630 Cre- control by one-sample t-test followed by Benjamini-Hochberg procedure with FDR set at
631 0.05. Proteins were only included in downstream analysis if they were significantly different
632 compared to Cre- control, had an average $\log_2$FC value > 0.58 compared to Cre- control, and all
633 individual LysoIP sample intensities were greater than no Cre control. Normalized abundances of
634 the Cre- controls were subtracted from the normalized abundances of each sample. Protein
635 quantities were log2 transformed, and the median quantity of protein intensities for each LysoIP
636 sample was subtracted from individual protein intensities to account for differences in cell number
637 and LysoIP efficiency. Differential protein abundance was determined using an ANOVA test
638 applied to the normalized protein quantities using limma [84, 85]. Correction for multiple testing
639 was performed using the Benjamini Hochberg method with an FDR set at 0.05. Any protein with
640 adjusted p-value < 0.05 was considered significant. Gene ontology analysis was performed using
641 ShinyGO [86] to compare LysoIP samples and Cre- controls or Metascape to compare *Grn* WT
642 and *Grn* KO LysoIP samples. For ShinyGO, all proteins detected in a single TMT-MS run were
643 used as background proteins to determine enrichment of lysosomal proteins. For Metascape, all
644 526 proteins detected as LysoIP proteins after filtering were included as background.
645
646 Western blotting
647 For STING activation assay, cell lysate was first normalized to match lowest concentration as
648 determined by Lowry assay. For all western blotting (except for Mfsd8 immunoblotting), 5x sample

649 buffer was added per sample, and samples were boiled at 95°C for 10 minutes. 10-14 µl per
650 sample was added to pre-cast gel, and electrophoresis was performed at 120V for 70-90 minutes.
651 Samples were transferred to 0.22 µm nitrocellulose membranes using Bio-Rad semi-dry transfer
652 (25V, 1.3-2.5A, 15 minutes). Membranes were blocked with 5% milk in TBS-T and incubated with
653 primary antibody in 3% BSA in TBS-T + 0.02% NaN_3 either at room temperature for 60 minutes
654 or overnight at 4°C. Membranes were rinsed in TBS-T, and secondary was applied for 60 minutes
655 in 5% milk TBS-T. Membranes were rinsed in TBS-T and either imaged using Licor or ECL.
656
657 For Mfsd8 immunoblotting, 5x sample buffer was added to samples and were heated at 37°C for
658 10 minutes. Samples were run on pre-cast gels as previously described and were transferred to
659 0.22 µm PVDF membranes using wet transfer apparatus (40V overnight at 4°C). Membranes
660 were blocked with 5% milk in TBS-T and incubated with primary antibody in 3% BSA in TBS-T +
661 0.02% NaN_3 overnight at 4°C. Membranes were rinsed in TBS-T, and secondary was applied for
662 60 minutes in 5% milk TBST. Membranes were rinsed in TBS-T and imaged using ECL.
663
664 Isolation of microglia
665 Microglia were isolated from *Grn;TMEM192-3xHA fl/fl;Cx3cr1-Cre^{ERT2}* was performed on 10-12-
666 month-old mice. Mice were anesthetized with isoflurane and perfused with ice cold PBS (10 mL
667 delivered over 4-5 minutes). Brain was harvested and left and right hemibrains were separated.
668 LysoIP was immediately performed on left hemibrain while right hemibrain was left in dissociation
669 buffer on ice. No more than 4 LysoIPs were performed before microglial isolation was performed.
670 To isolate single cell solution, hemibrains were dissociated by mincing tissue in dissociation buffer
671 on ice until no pieces larger than 1 mm remained. Tissue was moved to 50 mL conical tube and
672 rocked at 37°C for 30 minutes. Dissociated tissue was pressed through pre-wet 70 µm nylon filter
673 using rubber end of a syringe plunger. 2 mL sample preparation media was used to rinse
674 remaining cells through filter. Suspension was centrifuged for at 300g for 10 minutes at 4°C with

675 brake set to low. Supernatant was removed, and cell pellet was resuspended in 4 mL 30% percoll
676 solution. Solution was transferred to 15 mL conical tube and spun at 700g for 10 minutes at room
677 temperature with brake set to zero. Upper myelin layer was removed with 5 mL serologic pipette,
678 and remainder of supernatant was removed. Cells were resuspended in 1 mL sample preparation
679 media, and suspension was moved to fresh tube. Suspension was spun down at 300g for 10
680 minutes at 4°C with brake set to low. Supernatant was removed.
681
682 To isolate microglia, pellet was resuspended in 135 μL MACS buffer and 15 μL CD11b beads and
683 was incubated on ice for 15 minutes. 1 mL of MACS buffer was added, and sample was
684 centrifuged at 300g for 10 minutes at 4°C. 70 μm pre-wet nylon filter was placed on LS columns,
685 and both were attached to MACS magnetic stand. Column was prewet with 3 mL MACS buffer.
686 Supernatant was removed from pellet, and pellet was resuspended in 500 μL MACS buffer.
687 Sample was run over column. Tube was rinsed with 2 mL MACS buffer, and rinse was also run
688 over column. 3 mL MACS buffer was run over column.
689
690 Column was removed from magnet, 5 mL MACS buffer was added, and buffer was immediately
691 plunged into fresh tube. This was repeated with another 5 mL MACS buffer. This tube now
692 contained isolated microglia. Cells were spun at 300g for 10 minutes at 4°C with low brake.
693 Supernatant was removed, and pellet was resuspended in 50 μL lysis buffer.
694
695 <u>NAD+/NADH Assay</u>
696 Procedure is described on Abcam website for kit (Cat# ab65348). In brief, ~20 mg whole brain
697 from fasted mice was homogenized in 400 μL Extraction Buffer in Dounce homogenizer (40
698 passes). Samples were centrifuged for 5 minutes 4°C at top speed. Supernatant was passed
699 through a 10 kDa spin column (Millipore Sigma) 30 minutes 4°C at 14,000g to remove NAD-

700 consuming enzymes. Half of sample was reserved as “NAD Total” and half was heated at 60°C
701 for 30 minutes to degrade NAD+ (“NADH”). Added 50 µL sample to 100 µL reaction mix (98 µL
702 NAD cycling buffer + 2 uL NAD cycling enzyme) and incubated at room temp for 5 minutes to
703 convert NAD to NADH. 10 µL of developer solution was added, and colorimetric readout was
704 measured at OD 450 nm at multiple times between 1-4 hours. Samples were compared to 0-100
705 pmol NAD standards. NAD+ was calculated by subtracting NADH from NAD Total, and
706 NAD+/NADH ratios were calculated for each sample.
707
708 Seahorse Assay
709 To isolate mitochondria from 12-month-old *Grn* WT and Grn KO mice, mice were anesthetized
710 with isoflurane and perfused with cold PBS (5 mL over 4-5 minutes). Brains were extracted,
711 minced on ice, and placed in ~10 volumes of isolation buffer. Brains were homogenized by 2-3
712 slow strokes of a Dounce homogenizer. Sample was moved to fresh tube and spun at 800g for
713 10 minutes at 4°C. Supernatant was moved to fresh tube and spun at 8000g for 10 minutes at
714 4°C. Supernatant was removed, pellet was resuspended in 5 mL isolation buffer, and samples
715 were spun at 8000g for 10 minutes for 4°C. Supernatant was removed, and pellet containing
716 mitochondria was resuspended in 100 µL Seahorse buffer. Protein was quantified with BCA, and
717 mitochondria were diluted to a concentration of 100 µg protein/mL. 50 µL (5 µg)
718 mitochondria/sample was transferred to XFe24 Tissue Culture Plate. 4 wells contained 50 µL
719 Seahorse buffer alone as negative controls. Mitochondria were spun down onto plate surface at
720 3600g for 15 minutes at 4°C. 450 µL of starting buffer was added to each well while Seahorse is
721 calibrated according to manual. Starting buffers and injection port compounds are listed below.
722
723 Electron Flow Starting Buffer:
724 Seahorse Buffer + 10 mM pyruvate + 2 mM malate + 4 µM FCCP
725 Electron Flow Injection Ports:

726 Port A: 20 μM (10x) rotenone/injection volume 50 μL

727 Port B: 100 μM (10x) succinate/injection volume 55 μL

728 Port C: 40 μM (10x) actimycin A/injection volume 60 μL

729 Port D: 100mM (10x) ascorbate + 1 mM (10x) TMPD/injection volume 65 μL

730 Electron Coupling Starting Buffer:

731 Seahorse Buffer + 10 mM succinate + 2 μM rotenone

732 Port A: 40 mM (10x) ADP 50 μL

733 Port B: 20 μM (10x) oligomycin 55 μL

734 Port C: 40 μM (10x) FCCP/injection volume 60 μL

735 Port D: 40 μM (10x) antimycin A/injection volume 65 μL

736

737 Quantification and Statistical Analysis

738 Data analysis was conducted using ImageJ (NIH) and Odyssey Imaging Systems (Li-Cor).
739 GraphPad Prism was used for all statistical analysis except TMT-MS analysis which was
740 performed with the limma package which uses the R programming language. Data are displayed
741 as means ± standard errors (SE). Specific statistical tests including number of samples/condition
742 are specified in individual figure legends.

743

744 **Acknowledgments**

745 J. Herz was supported by grants from the NIA (RF1/RF3 AG053391), the NINDS and NIA (R01
746 NS093382 and R01 NS108115), NIAMS (1R43AR081762) and NINDS (1R43AG084450),
747 BrightFocus (A2013524S & A2016396S), the Bluefield Project to Cure FTD, Harrington Discovery
748 Institute (HDI2019-SI-4479), Alzheimer's Association (ABA-22-970304), the Presbyterian Village
749 North Foundation, and the Robert J. Kleberg Jr. & Helen C. Kleberg Foundation, Texas
750 Alzheimer's Research and Care Consortium (TARCC) 1271166 and 1280583. We also thank

Tamara Terrones, Brian Emmerson, and Patricia Strackbein for their unrivaled support and brilliant technical assistance.

Contributions

GCW and JH planned and conceived the project. GCW performed all experiments, analyzed data, and wrote the manuscript. JH edited the manuscript, obtained funding, and oversaw the execution of the project.

Declaration of Interests

J.H. is a co-founder of Reelin Therapeutics Inc. and coinventor of a patent related to isoxazoles with the ability to increase progranulin expression (Application Number: US15/127,603 and Publication Number: US10149836B2). The remaining authors declare no competing interest.

765 **References**

766 1. Bang, J., S. Spina, and B.L. Miller, *Frontotemporal dementia.* Lancet, 2015. **386**(10004):
767 p. 1672-82.

768 2. Ratnavalli, E., et al., *The prevalence of frontotemporal dementia.* Neurology, 2002. **58**(11):
769 p. 1615-21.

770 3. Baker, M., et al., *Mutations in progranulin cause tau-negative frontotemporal dementia*
771 *linked to chromosome 17.* Nature, 2006. **442**(7105): p. 916-9.

772 4. Rohrer, J.D., et al., *The heritability and genetics of frontotemporal lobar degeneration.*
773 Neurology, 2009. **73**(18): p. 1451-6.

774 5. Hu, F., et al., *Sortilin-mediated endocytosis determines levels of the frontotemporal*
775 *dementia protein, progranulin.* Neuron, 2010. **68**(4): p. 654-67.

776 6. Zhou, X., et al., *Prosaposin facilitates sortilin-independent lysosomal trafficking of*
777 *progranulin.* J Cell Biol, 2015. **210**(6): p. 991-1002.

778 7. Bai, X.H., et al., *ADAMTS-7, a direct target of PTHrP, adversely regulates endochondral*
779 *bone growth by associating with and inactivating GEP growth factor.* Mol Cell Biol, 2009.
780 **29**(15): p. 4201-19.

781 8. Kessenbrock, K., et al., *Proteinase 3 and neutrophil elastase enhance inflammation in*
782 *mice by inactivating antiinflammatory progranulin.* J Clin Invest, 2008. **118**(7): p. 2438-47.

783 9. Smith, K.R., et al., *Strikingly different clinicopathological phenotypes determined by*
784 *progranulin-mutation dosage.* Am J Hum Genet, 2012. **90**(6): p. 1102-7.

785 10. Valdez, C., et al., *Progranulin-mediated deficiency of cathepsin D results in FTD and NCL-*
786 *like phenotypes in neurons derived from FTD patients.* Hum Mol Genet, 2017. **26**(24): p.
787 4861-4872.

788 11. Zhou, X., et al., *Regulation of cathepsin D activity by the FTLD protein progranulin.* Acta
789 Neuropathol, 2017. **134**(1): p. 151-153.

790 12. Boland, S., et al., *Deficiency of the frontotemporal dementia gene GRN results in*
791 *gangliosidosis.* Nat Commun, 2022. **13**(1): p. 5924.
792 13. Evers, B.M., et al., *Lipidomic and Transcriptomic Basis of Lysosomal Dysfunction in*
793 *Progranulin Deficiency.* Cell Rep, 2017. **20**(11): p. 2565-2574.
794 14. Logan, T., et al., *Rescue of a lysosomal storage disorder caused by Grn loss of function*
795 *with a brain penetrant progranulin biologic.* Cell, 2021. **184**(18): p. 4651-4668 e25.
796 15. Tanaka, Y., et al., *Progranulin regulates lysosomal function and biogenesis through*
797 *acidification of lysosomes.* Hum Mol Genet, 2017. **26**(5): p. 969-988.
798 16. Tesla, R., et al., *Benzoxazole-derivatives enhance progranulin expression and reverse the*
799 *aberrant lysosomal proteome caused by GRN haploinsufficiency.* Nat Commun, 2024.
800 **15**(1): p. 6125.
801 17. Hasan, S., et al., *Multi-modal proteomic characterization of lysosomal function and*
802 *proteostasis in progranulin-deficient neurons.* Mol Neurodegener, 2023. **18**(1): p. 87.
803 18. Butler, V.J., et al., *Age- and stress-associated C. elegans granulins impair lysosomal*
804 *function and induce a compensatory HLH-30/TFEB transcriptional response.* PLoS Genet,
805 2019. **15**(8): p. e1008295.
806 19. Tanaka, Y., et al., *Increased lysosomal biogenesis in activated microglia and exacerbated*
807 *neuronal damage after traumatic brain injury in progranulin-deficient mice.* Neuroscience,
808 2013. **250**: p. 8-19.
809 20. Van Damme, P., et al., *Progranulin functions as a neurotrophic factor to regulate neurite*
810 *outgrowth and enhance neuronal survival.* J Cell Biol, 2008. **181**(1): p. 37-41.
811 21. Gass, J., et al., *Progranulin regulates neuronal outgrowth independent of sortilin.* Mol
812 Neurodegener, 2012. **7**: p. 33.
813 22. Lui, H., et al., *Progranulin Deficiency Promotes Circuit-Specific Synaptic Pruning by*
814 *Microglia via Complement Activation.* Cell, 2016. **165**(4): p. 921-35.

815 23. He, Z., et al., *Progranulin (PC-cell-derived growth factor/acrogranin) regulates invasion*
816 *and cell survival.* Cancer Res, 2002. **62**(19): p. 5590-6.
817 24. Gillett, D.A., et al., *Progranulin and GPNMB: interactions in endo-lysosome function and*
818 *inflammation in neurodegenerative disease.* J Neuroinflammation, 2023. **20**(1): p. 286.
819 25. Davis, S.E., et al., *Delivering progranulin to neuronal lysosomes protects against*
820 *excitotoxicity.* Journal of Biological Chemistry, 2021. **297**(3).
821 26. Zhang, J., et al., *Neurotoxic microglia promote TDP-43 proteinopathy in progranulin*
822 *deficiency.* Nature, 2020. **588**(7838): p. 459-465.
823 27. Laqtom, N.N., et al., *CLN3 is required for the clearance of glycerophosphodiesters from*
824 *lysosomes.* Nature, 2022. **609**(7929): p. 1005-1011.
825 28. Ghoochani, A., et al., *Cell-Type Resolved Protein Atlas of Brain Lysosomes Identifies*
826 *SLC45A1-Associated Disease as a Lysosomal Disorder.* bioRxiv, 2024.
827 29. Petkau, T.L., et al., *Progranulin expression in the developing and adult murine brain.* J
828 Comp Neurol, 2010. **518**(19): p. 3931-47.
829 30. Cawley, N.X., et al., *Abnormal LAMP1 glycosylation may play a role in Niemann-Pick*
830 *disease, type C pathology.* PLoS One, 2020. **15**(1): p. e0227829.
831 31. Ghossoub, R., et al., *Tetraspanin-6 negatively regulates exosome production.* Proc Natl
832 Acad Sci U S A, 2020. **117**(11): p. 5913-5922.
833 32. Lee, S.A., et al., *Functional expression of dopamine D2 receptor is regulated by*
834 *tetraspanin 7-mediated postendocytic trafficking.* FASEB J, 2017. **31**(6): p. 2301-2313.
835 33. Bassani, S., et al., *The X-linked intellectual disability protein TSPAN7 regulates excitatory*
836 *synapse development and AMPAR trafficking.* Neuron, 2012. **73**(6): p. 1143-58.
837 34. Salas, I.H., et al., *Tetraspanin 6: A novel regulator of hippocampal synaptic transmission*
838 *and long term plasticity.* PLoS One, 2017. **12**(2): p. e0171968.
839 35. Sukalskaia, A., et al., *Interactions between TTYH2 and APOE facilitate endosomal lipid*
840 *transfer.* Nature, 2025.

841 36. Reiman, E.M., V. Ghisays, and J.B. Langbaum, *The Risk of Alzheimer Disease in APOE4*
842 *Homozygotes.* JAMA Neurol, 2025. **82**(9): p. 879-880.
843 37. Ingannato, A., et al., *GRN Missense Variants and Familial Alzheimer's Disease: Two Case*
844 *Reports.* J Alzheimers Dis, 2023. **96**(2): p. 767-775.
845 38. Huang, M., et al., *Network analysis of the progranulin-deficient mouse brain proteome*
846 *reveals pathogenic mechanisms shared in human frontotemporal dementia caused by*
847 *GRN mutations.* Acta Neuropathol Commun, 2020. **8**(1): p. 163.
848 39. Singh, J., et al., *Systematic Comparison of Strategies for the Enrichment of Lysosomes*
849 *by Data Independent Acquisition.* Journal of Proteome Research, 2019. **19**(1): p. 371-381.
850 40. Bongarzone, E.R., et al., *Insights into the Pathogenesis and Treatment of Krabbe Disease.*
851 Pediatr Endocrinol Rev, 2016. **13 Suppl 1**: p. 689-96.
852 41. Brady, R.O., J. Kanfer, and D. Shapiro, *The Metabolism of Glucocerebrosides. I.*
853 *Purification and Properties of a Glucocerebroside-Cleaving Enzyme from Spleen Tissue.*
854 J Biol Chem, 1965. **240**: p. 39-43.
855 42. Senkevich, K., et al., *GALC variants affect galactosylceramidase enzymatic activity and*
856 *risk of Parkinson's disease.* Brain, 2023. **146**(5): p. 1859-1872.
857 43. Zhang, X., et al., *Clinical, mechanistic, biomarker, and therapeutic advances in GBA1-*
858 *associated Parkinson's disease.* Transl Neurodegener, 2024. **13**(1): p. 48.
859 44. Liu, G.Y. and D.M. Sabatini, *mTOR at the nexus of nutrition, growth, ageing and disease.*
860 Nat Rev Mol Cell Biol, 2020. **21**(4): p. 183-203.
861 45. Nader, W.O., et al., *TFEB overexpression alleviates autophagy-lysosomal deficits caused*
862 *by progranulin insufficiency.* Sci Rep, 2025. **15**(1): p. 26217.
863 46. Chang, M.C., et al., *Progranulin deficiency causes impairment of autophagy and TDP-43*
864 *accumulation.* J Exp Med, 2017. **214**(9): p. 2611-2628.
865 47. Shoshan-Barmatz, V., et al., *VDAC, a multi-functional mitochondrial protein regulating cell*
866 *life and death.* Mol Aspects Med, 2010. **31**(3): p. 227-85.

867 48. Humphries, A.D., et al., *Dissection of the mitochondrial import and assembly pathway for*
868 *human Tom40.* J Biol Chem, 2005. **280**(12): p. 11535-43.
869 49. Cardoso, R., et al., *APOEvarepsilon4-TOMM40L Haplotype Increases the Risk of Mild*
870 *Cognitive Impairment Conversion to Alzheimer's Disease.* J Alzheimers Dis, 2020. **78**(2):
871 p. 587-601.
872 50. Sen, A., et al., *Mitochondrial membrane proteins and VPS35 orchestrate selective removal*
873 *of mtDNA.* Nat Commun, 2022. **13**(1): p. 6704.
874 51. Rodriguez-Perinan, G., et al., *Progranulin Deficiency Induces Mitochondrial Dysfunction*
875 *in Frontotemporal Lobar Degeneration with TDP-43 Inclusions.* Antioxidants (Basel),
876 2023. **12**(3).
877 52. Zhou, D., et al., *PGRN acts as a novel regulator of mitochondrial homeostasis by*
878 *facilitating mitophagy and mitochondrial biogenesis to prevent podocyte injury in diabetic*
879 *nephropathy.* Cell Death Dis, 2019. **10**(7): p. 524.
880 53. Geier, E.G., et al., *Rare variants in the neuronal ceroid lipofuscinosis gene MFSD8 are*
881 *candidate risk factors for frontotemporal dementia.* Acta Neuropathol, 2019. **137**(1): p. 71-
882 88.
883 54. Siintola, E., et al., *The novel neuronal ceroid lipofuscinosis gene MFSD8 encodes a*
884 *putative lysosomal transporter.* Am J Hum Genet, 2007. **81**(1): p. 136-46.
885 55. Zampieri, S., et al., *SMPD1 Mutation Update: Database and Comprehensive Analysis of*
886 *Published and Novel Variants.* Hum Mutat, 2016. **37**(2): p. 139-47.
887 56. Elsea, S.H., et al., *ASAH1 pathogenic variants associated with acid ceramidase*
888 *deficiency: Farber disease and spinal muscular atrophy with progressive myoclonic*
889 *epilepsy.* Hum Mutat, 2020. **41**(9): p. 1469-1487.
890 57. Wang, X., et al., *Molecular mechanisms and targeted therapy of progranulin in metabolic*
891 *diseases.* Front Endocrinol (Lausanne), 2025. **16**: p. 1553794.

892 58. Singh, S., et al., *PLD3 and PLD4 synthesize S,S-BMP, a key phospholipid enabling lipid*
893 *degradation in lysosomes.* Cell, 2024. **187**(24): p. 6820-6834 e24.
894 59. Zhang, T., et al., *Progranulin deficiency results in sex-dependent alterations in microglia*
895 *in response to demyelination.* Acta Neuropathol, 2023. **146**(1): p. 97-119.
896 60. Hofmann, S.L., et al., *Neuronal ceroid lipofuscinoses caused by defects in soluble*
897 *lysosomal enzymes (CLN1 and CLN2).* Curr Mol Med, 2002. **2**(5): p. 423-37.
898 61. Reifschneider, A., et al., *Loss of TREM2 rescues hyperactivation of microglia, but not*
899 *lysosomal deficits and neurotoxicity in models of progranulin deficiency.* EMBO J, 2022.
900 **41**(4): p. e109108.
901 62. Pesamaa, I., et al., *A microglial activity state biomarker panel differentiates FTD-granulin*
902 *and Alzheimer's disease patients from controls.* Mol Neurodegener, 2023. **18**(1): p. 70.
903 63. Wang, A., et al., *Innate immune sensing of lysosomal dysfunction drives multiple*
904 *lysosomal storage disorders.* Nat Cell Biol, 2024. **26**(2): p. 219-234.
905 64. Chu, T.T., et al., *Tonic prime-boost of STING signalling mediates Niemann-Pick disease*
906 *type C.* Nature, 2021. **596**(7873): p. 570-575.
907 65. Chowdhury, S.R., et al., *PPT1 is a negative regulator of STING signaling in cancer cells*
908 *and its inhibition reactivates immune surveillance in cold tumors.* Proc Natl Acad Sci U S
909 A, 2025. **122**(39): p. e2514948122.
910 66. Ramanjulu, J.M., et al., *Design of amidobenzimidazole STING receptor agonists with*
911 *systemic activity.* Nature, 2018. **564**(7736): p. 439-443.
912 67. Xu, Y. and W. Wan, *Lysosomal control of the cGAS-STING signaling.* Trends Cell Biol,
913 2024. **34**(8): p. 622-625.
914 68. Hasan, S., et al., *Multi-modal Proteomic Characterization of Lysosomal Function and*
915 *Proteostasis in Progranulin-Deficient Neurons.* bioRxiv, 2023.
916 69. Zhou, X., et al., *Progranulin deficiency leads to reduced glucocerebrosidase activity.* PLoS
917 One, 2019. **14**(7): p. e0212382.

918 70. Boyle, N.R., et al., *Reduction of sphingomyelinase activity associated with progranulin*
919 *deficiency and frontotemporal dementia.* Neurobiol Dis, 2025. **213**: p. 107024.
920 71. Yang, C., et al., *sPLA2-IIA modifies progranulin deficiency phenotypes in mouse models.*
921 Mol Neurodegener, 2025. **20**(1): p. 72.
922 72. Bajaj, L., et al., *A CLN6-CLN8 complex recruits lysosomal enzymes at the ER for Golgi*
923 *transfer.* J Clin Invest, 2020. **130**(8): p. 4118-4132.
924 73. Devireddy, S. and S.M. Ferguson, *Efficient progranulin exit from the ER requires its*
925 *interaction with prosaposin, a Surf4 cargo.* J Cell Biol, 2022. **221**(2).
926 74. Udayar, V., et al., *Lysosomal dysfunction in neurodegeneration: emerging concepts and*
927 *methods.* Trends Neurosci, 2022. **45**(3): p. 184-199.
928 75. Gomez-Sintes, R., M.D. Ledesma, and P. Boya, *Lysosomal cell death mechanisms in*
929 *aging.* Ageing Res Rev, 2016. **32**: p. 150-168.
930 76. Sevigny, J., et al., *Progranulin AAV gene therapy for frontotemporal dementia: translational*
931 *studies and phase 1/2 trial interim results.* Nat Med, 2024. **30**(5): p. 1406-1415.
932 77. Kurnellas, M., et al., *Latozinemab, a novel progranulin-elevating therapy for*
933 *frontotemporal dementia.* J Transl Med, 2023. **21**(1): p. 387.
934 78. Rosenthal, Z.C., et al., *Epigenetic modulation through BET bromodomain inhibitors as a*
935 *novel therapeutic strategy for progranulin-deficient frontotemporal dementia.* Sci Rep,
936 2024. **14**(1): p. 9064.
937 79. Root, J., et al., *Granulins rescue inflammation, lysosome dysfunction, lipofuscin, and*
938 *neuropathology in a mouse model of progranulin deficiency.* Cell Rep, 2024. **43**(12): p.
939 114985.
940 80. Selkoe, D.J. and J. Hardy, *The amyloid hypothesis of Alzheimer's disease at 25 years.*
941 EMBO Mol Med, 2016. **8**(6): p. 595-608.
942 81. Morris, H.R., et al., *The pathogenesis of Parkinson's disease.* Lancet, 2024. **403**(10423):
943 p. 293-304.

944 82. Benussi, A., et al., *Conceptual framework for the definition of preclinical and prodromal*
945 *frontotemporal dementia.* Alzheimers Dement, 2022. **18**(7): p. 1408-1423.
946 83. Frew, J. and H.B. Nygaard, *Neuropathological and behavioral characterization of aged*
947 *Grn R493X progranulin-deficient frontotemporal dementia knockin mice.* Acta Neuropathol
948 Commun, 2021. **9**(1): p. 57.
949 84. Phipson, B., et al., *Robust Hyperparameter Estimation Protects against Hypervariable*
950 *Genes and Improves Power to Detect Differential Expression.* Ann Appl Stat, 2016. **10**(2):
951 p. 946-963.
952 85. Ritchie, M.E., et al., *limma powers differential expression analyses for RNA-sequencing*
953 *and microarray studies.* Nucleic Acids Res, 2015. **43**(7): p. e47.
954 86. Ge, S.X., D. Jung, and R. Yao, *ShinyGO: a graphical gene-set enrichment tool for animals*
955 *and plants.* Bioinformatics, 2020. **36**(8): p. 2628-2629.

956

957

958 **Table 1**

Gene Name	OMIM#	Disease	Log_2FC (*Grn* KO/*Grn* WT)
Abca2	600047	Intellectual developmental disorder with poor growth and with or without seizures or ataxia	-1.422
Abcd4	603214	Methylmalonic aciduria and homocystinuria, cblJ type	1.2586
Arsa	607574	Metachromatic leukodystrophy	-0.3898
Arsb	611542	Mucopolysaccharidosis type VI (Maroteaux-Lamy)	-0.3096
Arsg	610008	Usher syndrome, type IV	-1.14
Asah1	613468	Farber lipogranulomatosis	-0.8072
Atp6v0c	108745	Epilepsy, early-onset, 3, with or without developmental delay	1.424
Clcn6	602726	Ceroid lipofuscinosis, neuronal, 15	-0.5394
Ctsa	613111	Galactosialidosis	0.3282
Ctsc	602365	Haim-Munk syndrome	1.958
Dnase2	126350	Autoinflammatory-pancytopenia syndrome	1.35
Fuca1	612280	Fucosidosis	0.4864
Galc	606890	Krabbe disease	-0.6264
Gba1	606463	Gaucher Disease	-0.5804
Gm2a	613109	GM2-gangliosidosis, AB variant	0.3804
Grn	138945	Ceroid lipofuscinosis, neuronal, 11	-4.226

Hexb	606873	Sandhoff disease, infantile, juvenile, and adult forms	0.6222
Hgsnat	610453	Mucopolysaccharidosis type IIIC (Sanfilippo C)	0.8754
Ids	300823	Mucopolysaccharidosis II	-0.5634
Lamp2	309060	Danon disease	0.7078
Lipa	613497	Cholesteryl ester storage disease	0.2158
Mfsd8	611124	Ceroid lipofuscinosis, neuronal, 7	-2.568
Pld3	615698	Spinocerebellar ataxia 46	-0.5342
Ppt1	600722	Ceroid lipofuscinosis, neuronal, 1	-0.9972
Rab7a	602298	Charcot-Marie-Tooth disease, type 2B	1.28
Scarb2	602257	Epilepsy, progressive myoclonic 4, with or without renal failure	0.7028
Smpd1	607608	Niemann-Pick disease, type A/B	-1.222
Sod1	147450	Parkinson's Disease	0.3346
Tmem165	614726	Congenital disorder of glycosylation, type IIk	-1.1058
Tmem63a	618685	Leukodystrophy, hypomyelinating, 19, transient infantile	-1.368
Tpp1	607998	Ceroid lipofuscinosis, neuronal, 2	1.0158
Vps33a	610034	Mucopolysaccharidosis-plus syndrome	-0.371

959

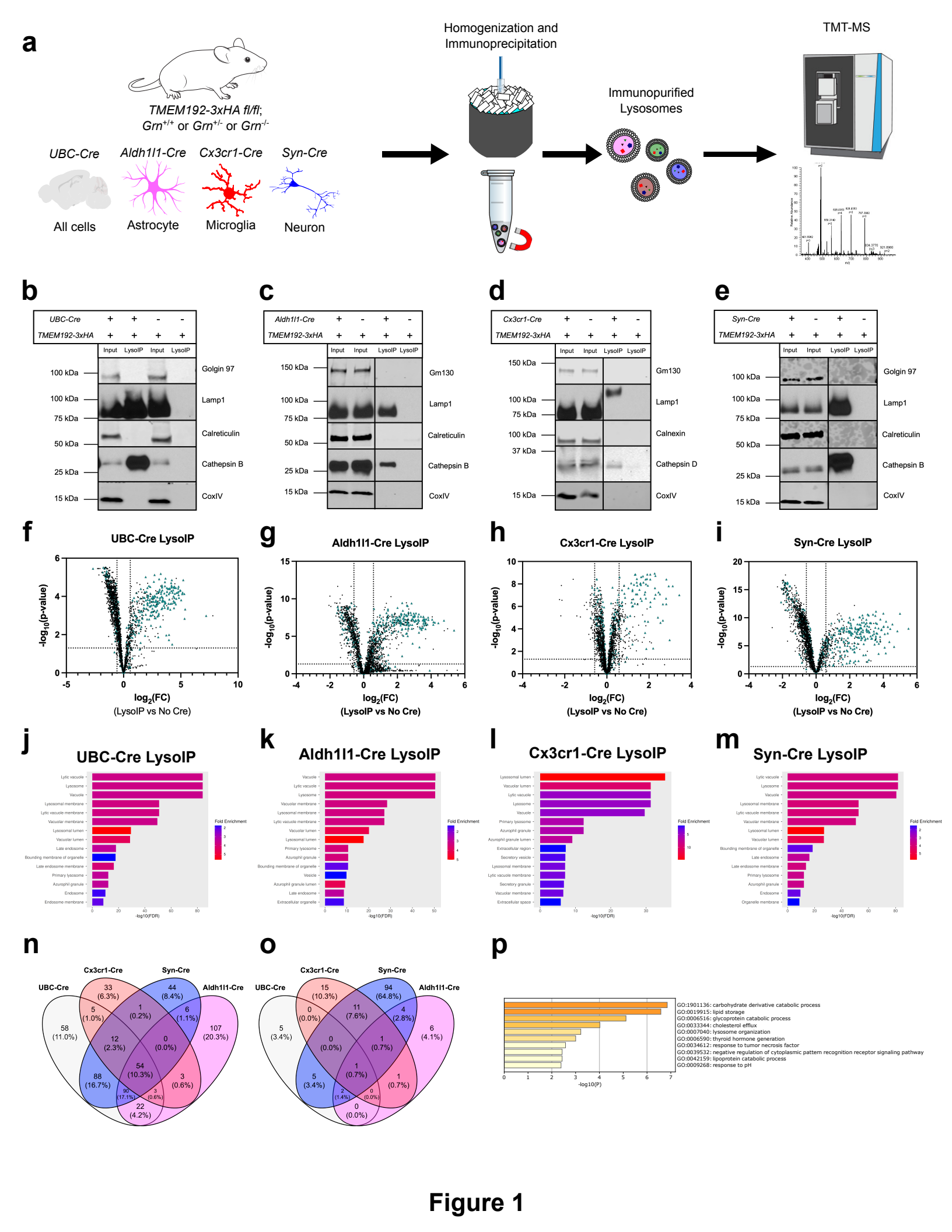
a
TMEM192-3xHA fl/fl;
Grn+/+ or Grn+/- or Grn-/-
UBC-Cre
Aldh1l1-Cre
Cx3cr1-Cre
Syn-Cre
All cells
Astrocyte
Microglia
Neuron
Homogenization and Immunoprecipitation
Immunopurified Lysosomes
TMT-MS
b
UBC-Cre
TMEM192-3xHA
Input LysoIP Input LysoIP
100 kDa Golgin 97
100 kDa Lamp1
75 kDa Calreticulin
50 kDa Cathepsin B
25 kDa CoxIV
15 kDa
c
Aldh1l1-Cre
TMEM192-3xHA
Input Input LysoIP LysoIP
150 kDa Gm130
100 kDa Lamp1
75 kDa Calreticulin
50 kDa Cathepsin B
25 kDa CoxIV
15 kDa
d
Cx3cr1-Cre
TMEM192-3xHA
Input Input LysoIP LysoIP
150 kDa Gm130
100 kDa Lamp1
75 kDa
100 kDa Calnexin
37 kDa Cathepsin D
15 kDa CoxIV
e
Syn-Cre
TMEM192-3xHA
Input Input LysoIP LysoIP
100 kDa Golgin 97
100 kDa Lamp1
75 kDa Calreticulin
50 kDa Cathepsin B
25 kDa CoxIV
15 kDa
f
UBC-Cre LysoIP
-log10(p-value)
log2(FC)
(LysoIP vs No Cre)
g
Aldh1l1-Cre LysoIP
-log10(p-value)
log2(FC)
(LysoIP vs No Cre)
h
Cx3cr1-Cre LysoIP
-log10(p-value)
log2(FC)
(LysoIP vs No Cre)
i
Syn-Cre LysoIP
-log10(p-value)
log2(FC)
(LysoIP vs No Cre)
j
UBC-Cre LysoIP
Lytic vacuole
Lysosome
Vacuole
Lysosomal membrane
Lytic vacuole membrane
Vacuolar membrane
Lysosomal lumen
Vacuolar lumen
Late endosome
Bounding membrane of organelle
Late endosome membrane
Primary lysosome
Azurophil granule
Endosome
Endosome membrane
Fold Enrichment
-log10(FDR)
k
Aldh1l1-Cre LysoIP
Vacuole
Lytic vacuole
Lysosome
Vacuolar membrane
Lysosomal membrane
Lytic vacuole membrane
Vacuolar lumen
Lysosomal lumen
Primary lysosome
Azurophil granule
Bounding membrane of organelle
Vesicle
Azurophil granule lumen
Late endosome
Extracellular organelle
Fold Enrichment
-log10(FDR)
l
Cx3cr1-Cre LysoIP
Lysosomal lumen
Vacuolar lumen
Lytic vacuole
Lysosome
Vacuole
Primary lysosome
Azurophil granule
Azurophil granule lumen
Extracellular region
Secretory vesicle
Lysosomal membrane
Lytic vacuole membrane
Secretory granule
Vacuolar membrane
Extracellular space
Fold Enrichment
-log10(FDR)
m
Syn-Cre LysoIP
Lytic vacuole
Lysosome
Vacuole
Lysosomal membrane
Lytic vacuole membrane
Vacuolar membrane
Lysosomal lumen
Vacuolar lumen
Bounding membrane of organelle
Late endosome
Late endosome membrane
Primary lysosome
Azurophil granule
Endosome
Organelle membrane
Fold Enrichment
-log10(FDR)
n
UBC-Cre
Cx3cr1-Cre
Syn-Cre
Aldh1l1-Cre
58 (11.0%)
33 (6.3%)
44 (8.4%)
107 (20.3%)
5 (1.0%)
1 (0.2%)
6 (1.1%)
12 (2.3%)
0 (0.0%)
54 (10.3%)
88 (16.7%)
3 (0.6%)
90 (17.1%)
3 (0.6%)
22 (4.2%)
o
UBC-Cre
Cx3cr1-Cre
Syn-Cre
Aldh1l1-Cre
5 (3.4%)
15 (10.3%)
94 (64.8%)
6 (4.1%)
0 (0.0%)
11 (7.6%)
4 (2.8%)
0 (0.0%)
1 (0.7%)
1 (0.7%)
5 (3.4%)
2 (1.4%)
0 (0.0%)
1 (0.7%)
0 (0.0%)
p
GO:1901136: carbohydrate derivative catabolic process
GO:0019915: lipid storage
GO:0006516: glycoprotein catabolic process
GO:0033344: cholesterol efflux
GO:0007040: lysosome organization
GO:0006590: thyroid hormone generation
GO:0034612: response to tumor necrosis factor
GO:0039532: negative regulation of cytoplasmic pattern recognition receptor signaling pathway
GO:0042159: lipoprotein catabolic process
GO:0009268: response to pH
-log10(P)

Figure 1

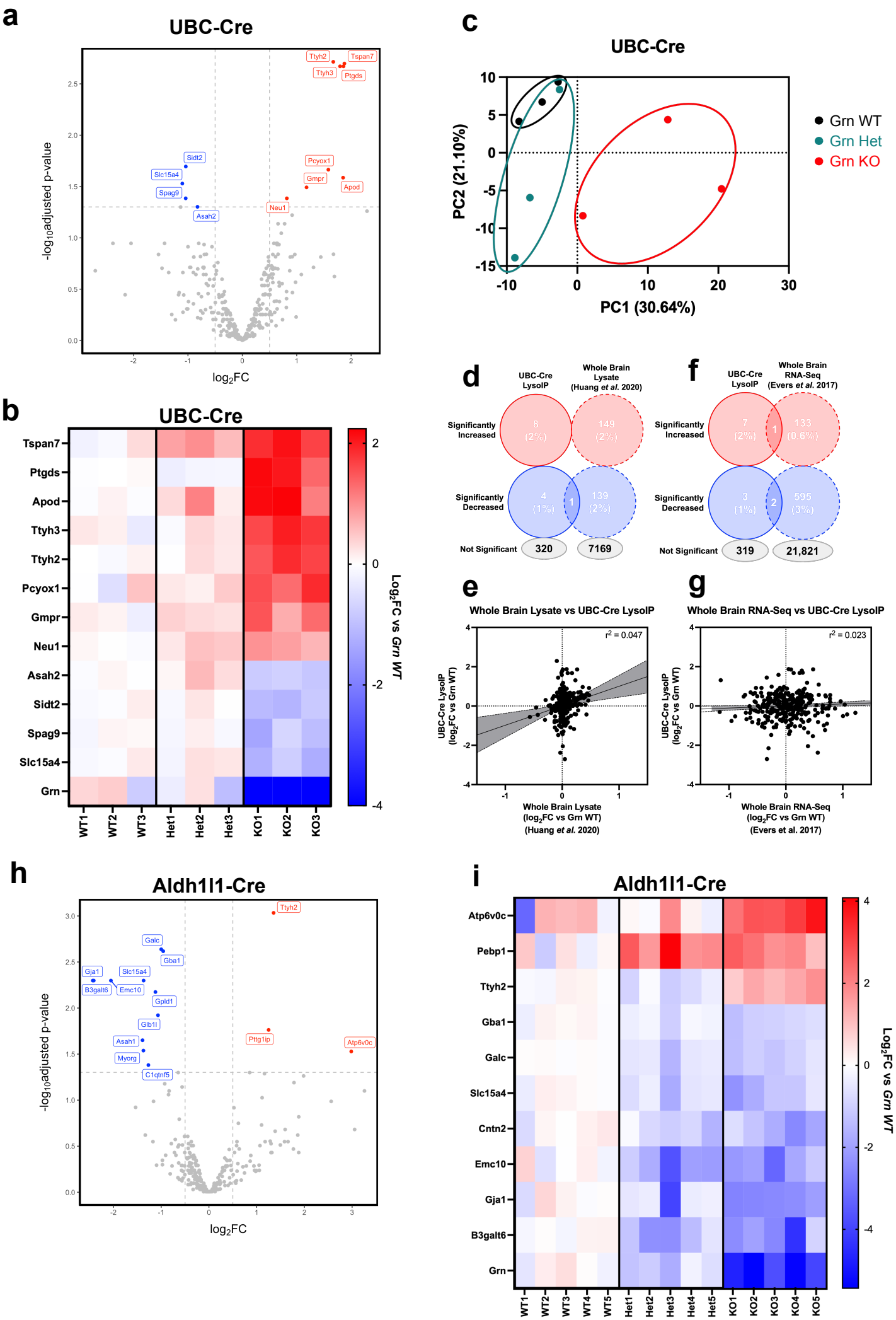
a
UBC-Cre
Ttyh2
Tspan7
Ttyh3
Ptgds
Sidt2
Slc15a4
Spag9
Asah2
Pcyox1
Gmpr
Apod
Neu1
-log10adjusted p-value
log2FC
b
UBC-Cre
Tspan7
Ptgds
Apod
Ttyh3
Ttyh2
Pcyox1
Gmpr
Neu1
Asah2
Sidt2
Spag9
Slc15a4
Grn
WT1
WT2
WT3
Het1
Het2
Het3
KO1
KO2
KO3
Log2FC vs Grn WT
c
UBC-Cre
PC2 (21.10%)
PC1 (30.64%)
Grn WT
Grn Het
Grn KO
d
UBC-Cre LysoIP
Whole Brain Lysate (Huang et al. 2020)
Significantly Increased
Significantly Decreased
Not Significant
8 (2%)
149 (2%)
4 (1%)
1
139 (2%)
320
7169
f
UBC-Cre LysoIP
Whole Brain RNA-Seq (Evers et al. 2017)
Significantly Increased
Significantly Decreased
Not Significant
7 (2%)
1
133 (0.6%)
3 (1%)
2
595 (3%)
319
21,821
e
Whole Brain Lysate vs UBC-Cre LysoIP
r2 = 0.047
UBC-Cre LysoIP (log2FC vs Grn WT)
Whole Brain Lysate (log2FC vs Grn WT) (Huang et al. 2020)
g
Whole Brain RNA-Seq vs UBC-Cre LysoIP
r2 = 0.023
UBC-Cre LysoIP (log2FC vs Grn WT)
Whole Brain RNA-Seq (log2FC vs Grn WT) (Evers et al. 2017)
h
Aldh1l1-Cre
Ttyh2
Galc
Gba1
Gja1
Slc15a4
B3galt6
Emc10
Gpld1
Glb1l
Asah1
Myorg
C1qtnf5
Pttg1ip
Atp6v0c
-log10adjusted p-value
log2FC
i
Aldh1l1-Cre
Atp6v0c
Pebp1
Ttyh2
Gba1
Galc
Slc15a4
Cntn2
Emc10
Gja1
B3galt6
Grn
WT1
WT2
WT3
WT4
WT5
Het1
Het2
Het3
Het4
Het5
KO1
KO2
KO3
KO4
KO5
Log2FC vs Grn WT

Figure 2

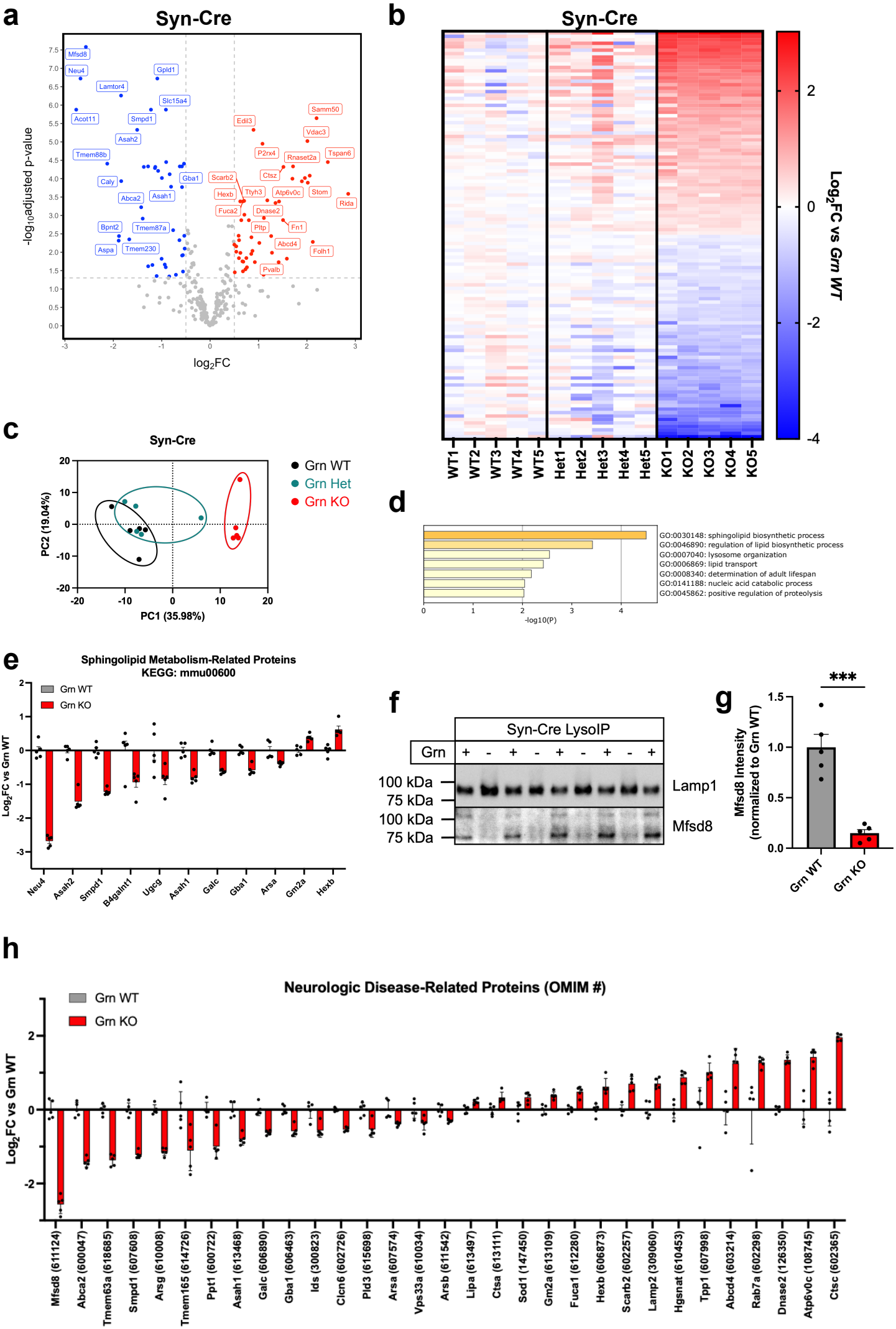
a
Syn-Cre
-log10adjusted p-value
log2FC
Mfsd8
Neu4
Gpld1
Lamtor4
Slc15a4
Acot11
Smpd1
Asah2
Tmem88b
Caly
Gba1
Abca2
Asah1
Bpnt2
Tmem87a
Aspa
Tmem230
Samm50
Edil3
Vdac3
P2rx4
Rnaset2a
Tspan6
Ctsz
Scarb2
Hexb
Ttyh3
Atp6v0c
Stom
Rida
Fuca2
Dnase2
Pltp
Fn1
Abcd4
Folh1
Pvalb
b
Syn-Cre
Log2FC vs Grn WT
WT1
WT2
WT3
WT4
WT5
Het1
Het2
Het3
Het4
Het5
KO1
KO2
KO3
KO4
KO5
c
Syn-Cre
Grn WT
Grn Het
Grn KO
PC2 (19.04%)
PC1 (35.98%)
d
GO:0030148: sphingolipid biosynthetic process
GO:0046890: regulation of lipid biosynthetic process
GO:0007040: lysosome organization
GO:0006869: lipid transport
GO:0008340: determination of adult lifespan
GO:0141188: nucleic acid catabolic process
GO:0045862: positive regulation of proteolysis
-log10(P)
e
Sphingolipid Metabolism-Related Proteins
KEGG: mmu00600
Grn WT
Grn KO
Log2FC vs Grn WT
Neu4
Asah2
Smpd1
B4galnt1
Ugcg
Asah1
Galc
Gba1
Arsa
Gm2a
Hexb
f
Syn-Cre LysoIP
Grn
100 kDa
75 kDa
100 kDa
75 kDa
Lamp1
Mfsd8
g
***
Mfsd8 Intensity
(normalized to Grn WT)
Grn WT
Grn KO
h
Neurologic Disease-Related Proteins (OMIM #)
Grn WT
Grn KO
Log2FC vs Grn WT
Mfsd8 (611124)
Abca2 (600047)
Tmem63a (618685)
Smpd1 (607608)
Arsg (610008)
Tmem165 (614726)
Ppt1 (600722)
Asah1 (613468)
Galc (606890)
Gba1 (606463)
Ids (300823)
Clcn6 (602726)
Pld3 (615698)
Arsa (607574)
Vps33a (610034)
Arsb (611542)
Lipa (613497)
Ctsa (613111)
Sod1 (147450)
Gm2a (613109)
Fuca1 (612280)
Hexb (606873)
Scarb2 (602257)
Lamp2 (309060)
Hgsnat (610453)
Tpp1 (607998)
Abcd4 (603214)
Rab7a (602298)
Dnase2 (126350)
Atp6v0c (108745)
Ctsc (602365)

Figure 3

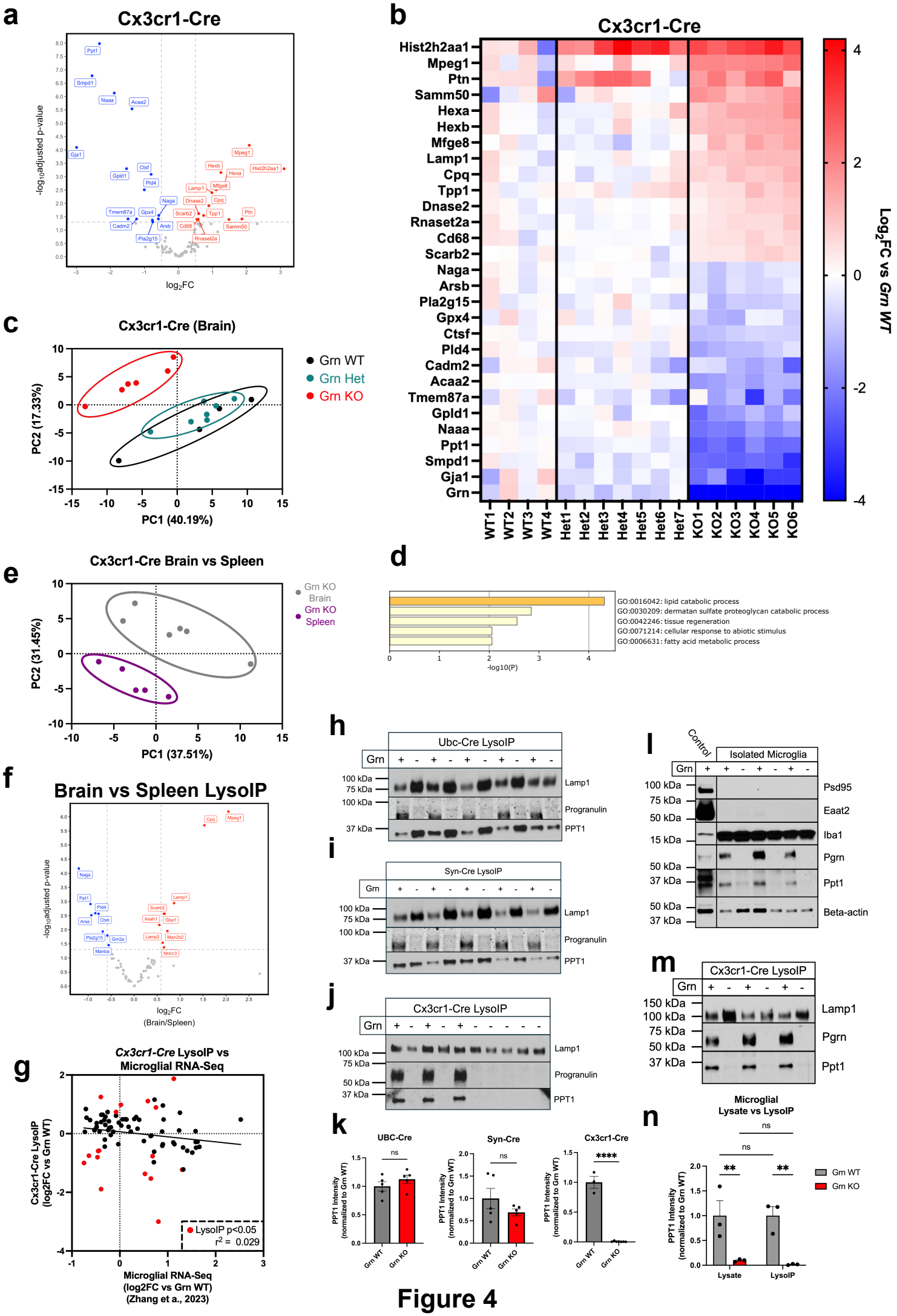
a
Cx3cr1-Cre
-log10adjusted p-value
log2FC
b
Cx3cr1-Cre
Hist2h2aa1
Mpeg1
Ptn
Samm50
Hexa
Hexb
Mfge8
Lamp1
Cpq
Tpp1
Dnase2
Rnaset2a
Cd68
Scarb2
Naga
Arsb
Pla2g15
Gpx4
Ctsf
Pld4
Cadm2
Acaa2
Tmem87a
Gpld1
Naaa
Ppt1
Smpd1
Gja1
Grn
WT1 WT2 WT3 WT4 Het1 Het2 Het3 Het4 Het5 Het6 Het7 KO1 KO2 KO3 KO4 KO5 KO6
Log2FC vs Grn WT
c
Cx3cr1-Cre (Brain)
PC2 (17.33%)
PC1 (40.19%)
Grn WT
Grn Het
Grn KO
d
GO:0016042: lipid catabolic process
GO:0030209: dermatan sulfate proteoglycan catabolic process
GO:0042246: tissue regeneration
GO:0071214: cellular response to abiotic stimulus
GO:0006631: fatty acid metabolic process
-log10(P)
e
Cx3cr1-Cre Brain vs Spleen
PC2 (31.45%)
PC1 (37.51%)
Grn KO Brain
Grn KO Spleen
f
Brain vs Spleen LysoIP
-log10adjusted p-value
log2FC
(Brain/Spleen)
g
Cx3cr1-Cre LysoIP vs Microglial RNA-Seq
Cx3cr1-Cre LysoIP (log2FC vs Grn WT)
Microglial RNA-Seq (log2FC vs Grn WT) (Zhang et a., 2023)
LysoIP p<0.05
r2 = 0.029
h
Ubc-Cre LysoIP
Grn
100 kDa
75 kDa
100 kDa
37 kDa
Lamp1
Progranulin
PPT1
i
Syn-Cre LysoIP
j
Cx3cr1-Cre LysoIP
150 kDa
50 kDa
l
Control
Isolated Microglia
Psd95
Eaat2
Iba1
Pgrn
Ppt1
Beta-actin
m
Cx3cr1-Cre LysoIP
k
UBC-Cre
Syn-Cre
Cx3cr1-Cre
PPT1 Intensity (normalized to Grn WT)
ns
****
Grn WT
Grn KO
n
Microglial Lysate vs LysoIP
Lysate
LysoIP
**

Figure 4

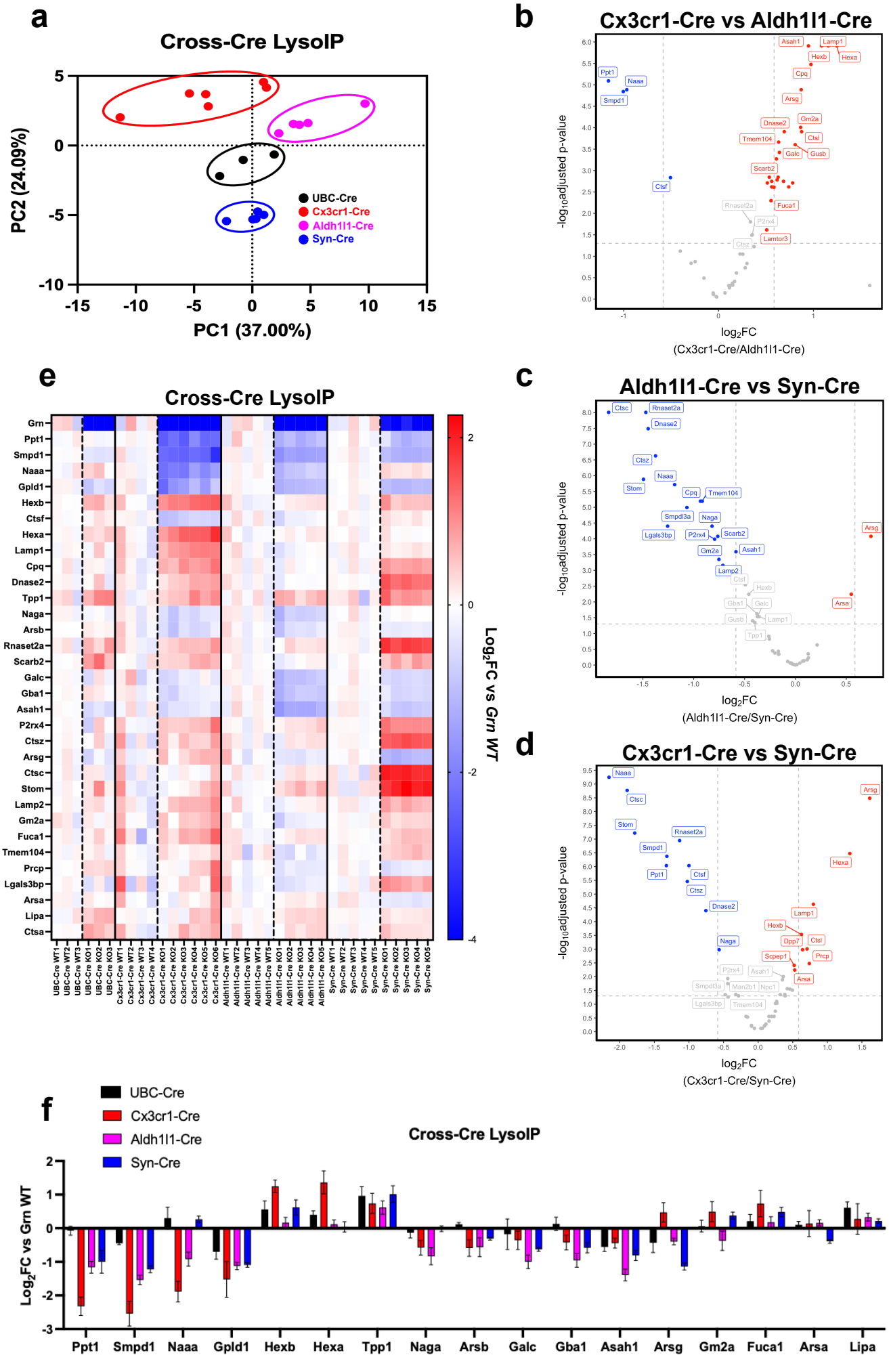
a
Cross-Cre LysoIP
PC2 (24.09%)
PC1 (37.00%)
UBC-Cre
Cx3cr1-Cre
Aldh1l1-Cre
Syn-Cre
b
Cx3cr1-Cre vs Aldh1l1-Cre
-log10adjusted p-value
log2FC
(Cx3cr1-Cre/Aldh1l1-Cre)
c
Aldh1l1-Cre vs Syn-Cre
-log10adjusted p-value
log2FC
(Aldh1l1-Cre/Syn-Cre)
d
Cx3cr1-Cre vs Syn-Cre
-log10adjusted p-value
log2FC
(Cx3cr1-Cre/Syn-Cre)
e
Cross-Cre LysoIP
Log2FC vs Grn WT
f
UBC-Cre
Cx3cr1-Cre
Aldh1l1-Cre
Syn-Cre
Cross-Cre LysoIP
Log2FC vs Grn WT
Ppt1
Smpd1
Naaa
Gpld1
Hexb
Hexa
Tpp1
Naga
Arsb
Galc
Gba1
Asah1
Arsg
Gm2a
Fuca1
Arsa
Lipa

Figure 5

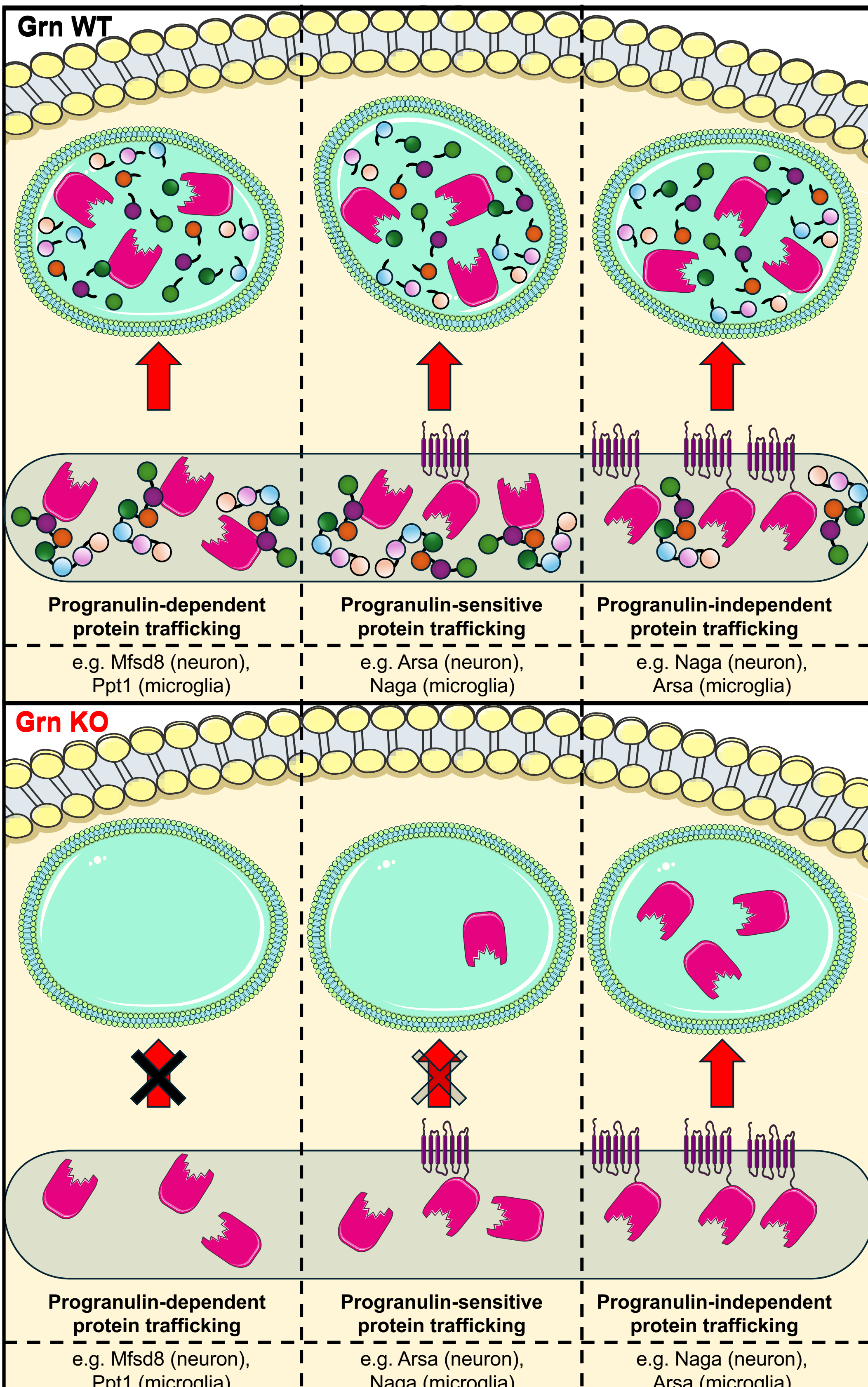
Grn WT
Progranulin-dependent protein trafficking
Progranulin-sensitive protein trafficking
Progranulin-independent protein trafficking
e.g. Mfsd8 (neuron), Ppt1 (microglia)
e.g. Arsa (neuron), Naga (microglia)
e.g. Naga (neuron), Arsa (microglia)
Grn KO
Progranulin-dependent protein trafficking
Progranulin-sensitive protein trafficking
Progranulin-independent protein trafficking
e.g. Mfsd8 (neuron), Ppt1 (microglia)
e.g. Arsa (neuron), Naga (microglia)
e.g. Naga (neuron), Arsa (microglia)

Figure 6

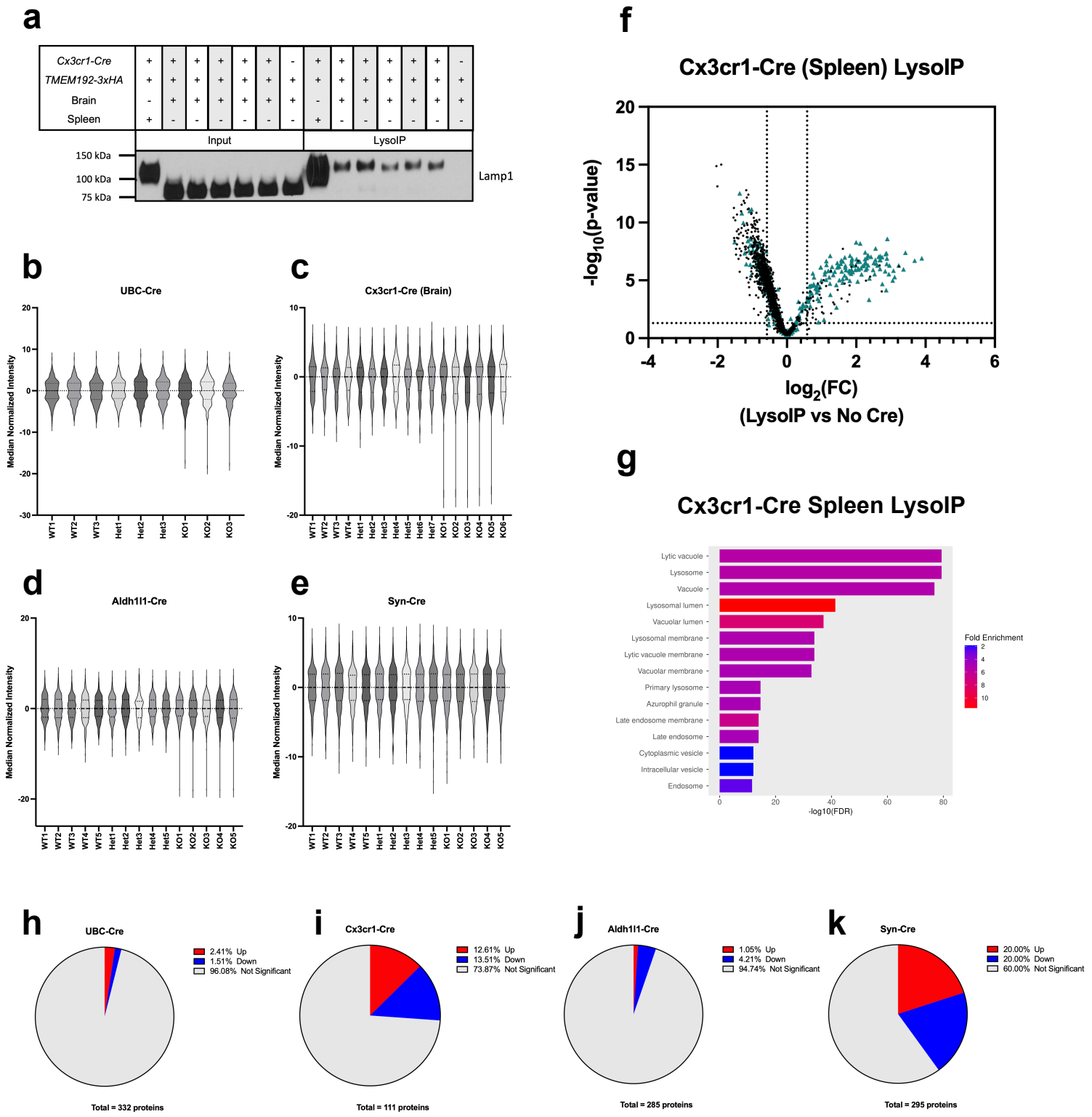

Supplemental Figure 1

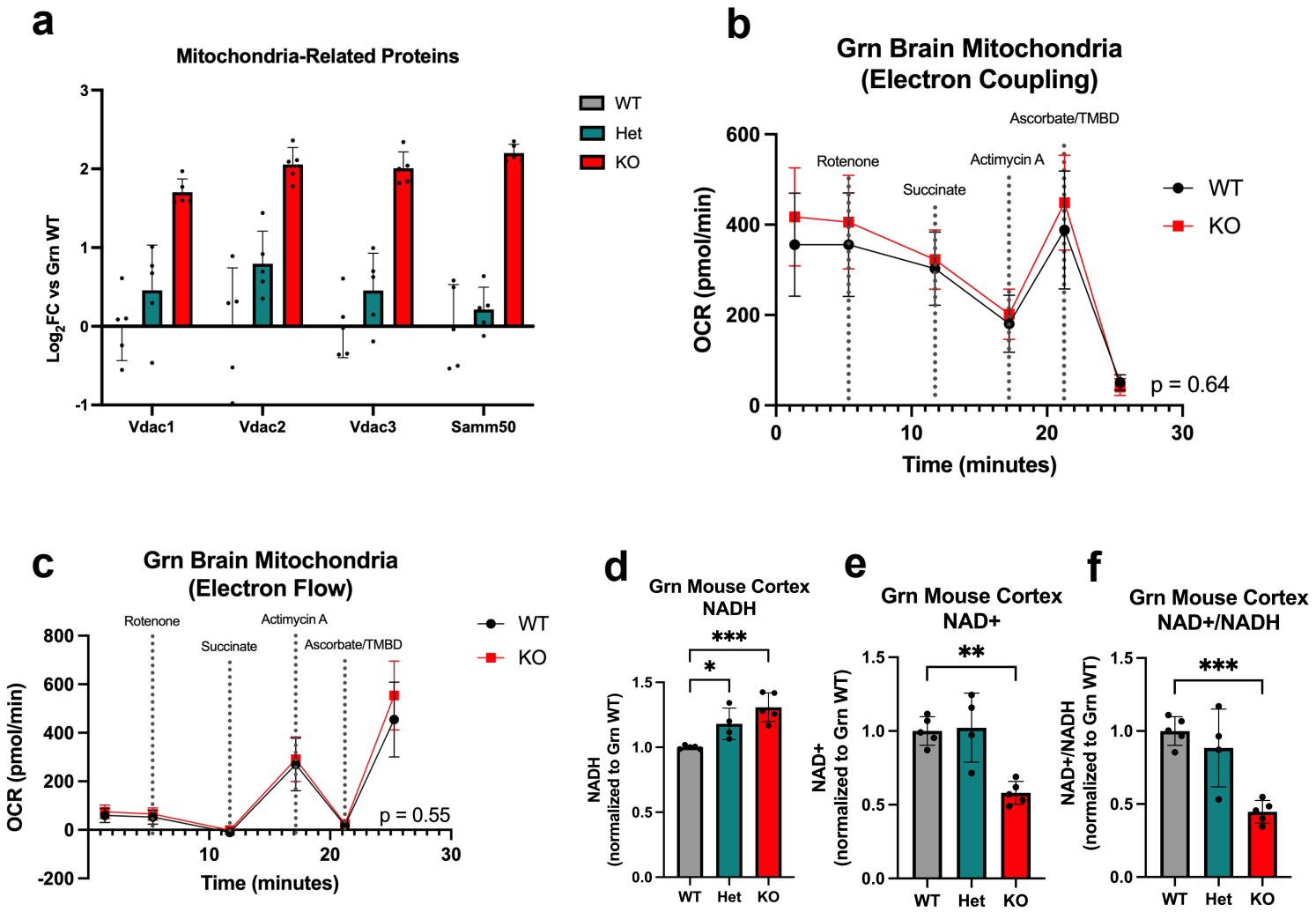

Supplemental Figure 2

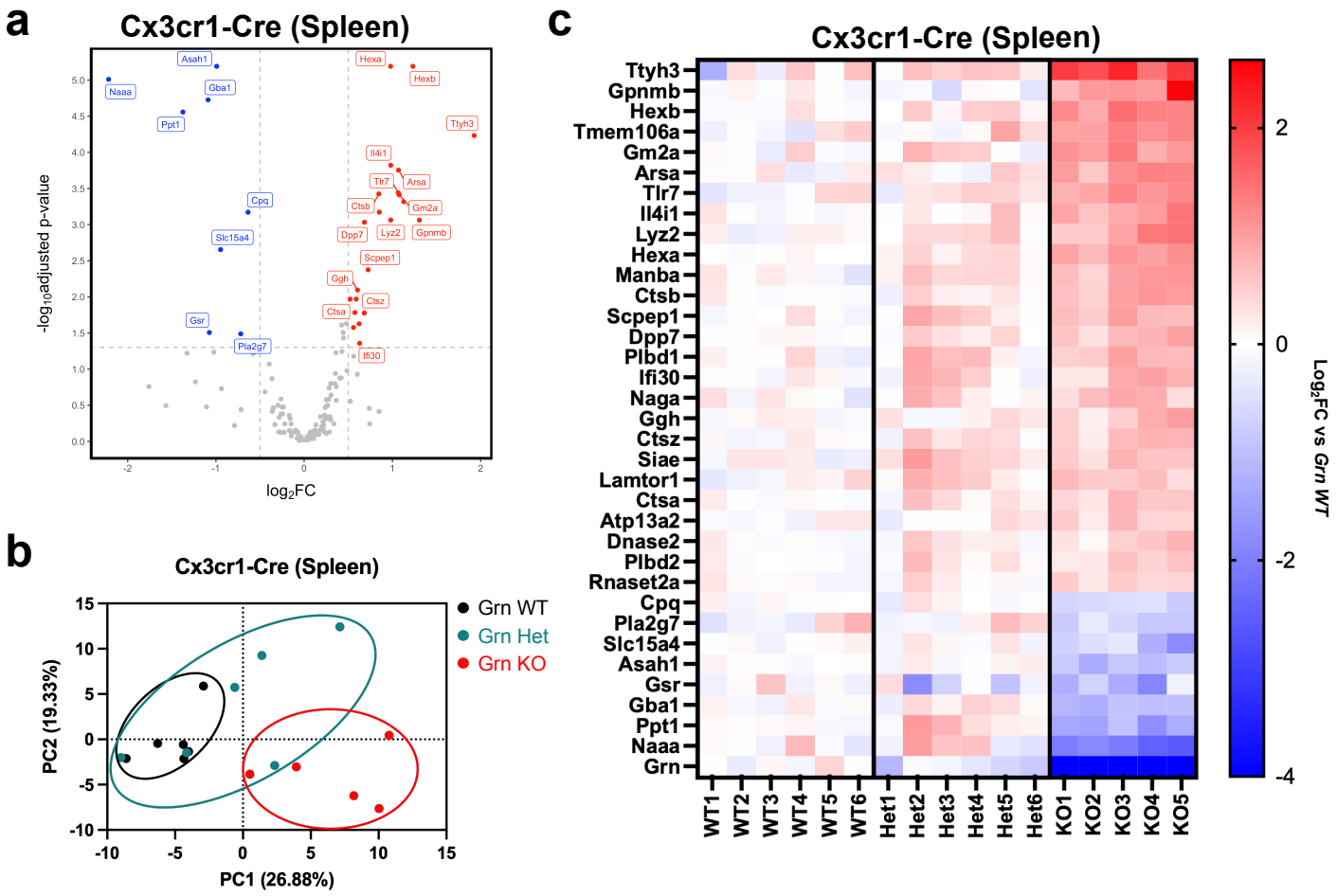

Supplemental Figure 3

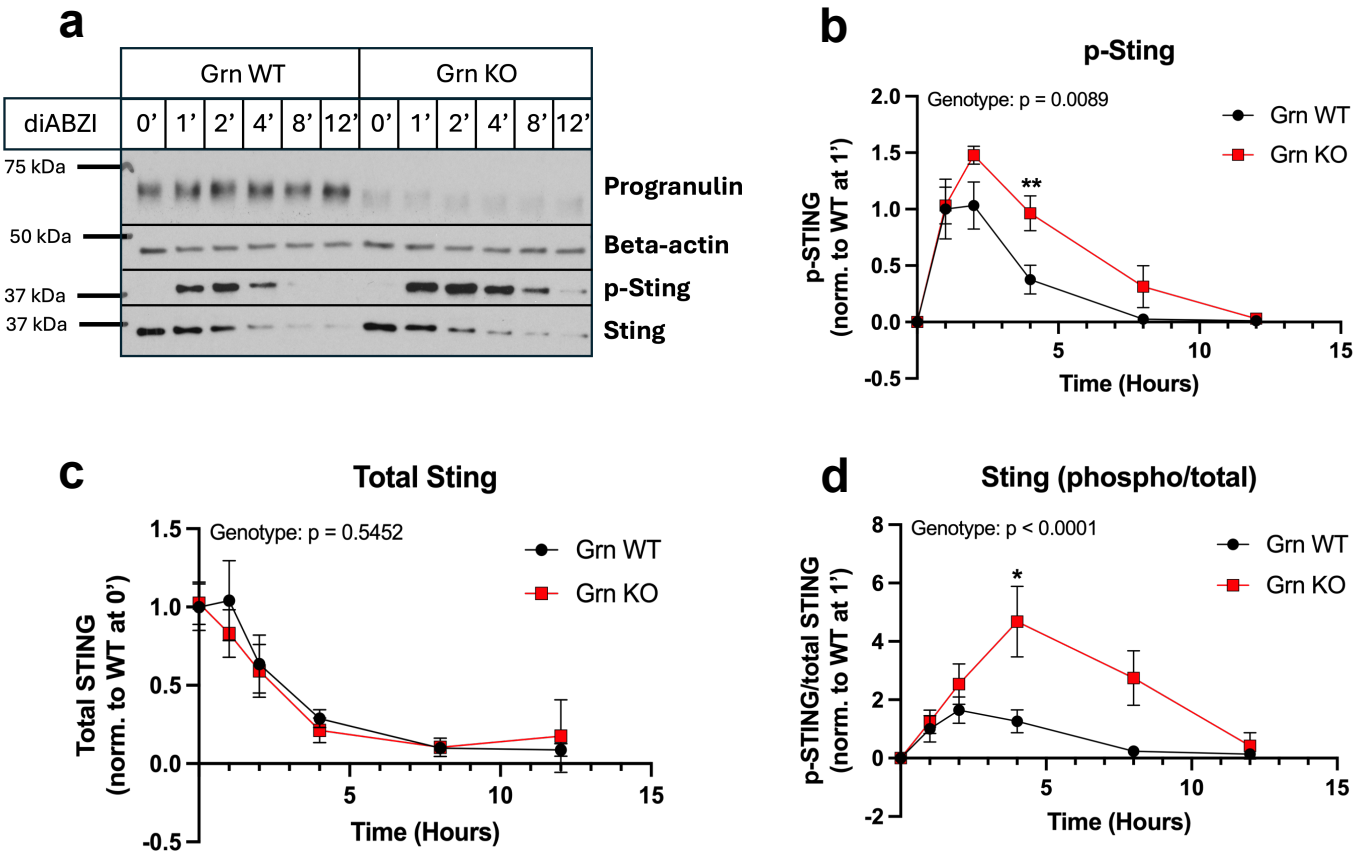

Supplemental Figure 4